A mechanosensitive peri-arteriolar niche for osteogenesis and lymphopoiesis

https://doi.org/10.1038/s41586-021-03298-5

Received: 20 April 2020

Accepted: 27 January 2021

Published online: 24 February 2021

Check for updates

Bo Shen[1], Alpaslan Tasdogan[1], Jessalyn M. Ubellacker[1], Jingzhu Zhang[1], Elena D. Nosyreva[2], Liming Du[1], Malea M. Murphy[1], Shuiqing Hu[3], Yating Yi[4], Nergis Kara[1], Xin Liu[1], Shay Guela[1], Yuemeng Jia[1], Vijayashree Ramesh[1], Claire Embree[1], Evann C. Mitchell[1], Yunduo C. Zhao[5], Lining A. Ju[5], Zhao Hu[5], Genevieve M. Crane[6], Zhiyu Zhao[1], Ruhma Syeda[3] & Sean J. Morrison[1,7]✉

Stromal cells in adult bone marrow that express leptin receptor (LEPR) are a critical source of growth factors, including stem cell factor (SCF), for the maintenance of haematopoietic stem cells and early restricted progenitors[1–6]. LEPR$^+$ cells are heterogeneous, including skeletal stem cells and osteogenic and adipogenic progenitors[7–12], although few markers have been available to distinguish these subsets or to compare their functions. Here we show that expression of an osteogenic growth factor, osteolectin[13,14], distinguishes peri-arteriolar LEPR$^+$ cells poised to undergo osteogenesis from peri-sinusoidal LEPR$^+$ cells poised to undergo adipogenesis (but retaining osteogenic potential). Peri-arteriolar LEPR$^+$osteolectin$^+$ cells are rapidly dividing, short-lived osteogenic progenitors that increase in number after fracture and are depleted during ageing. Deletion of *Scf* from adult osteolectin$^+$ cells did not affect the maintenance of haematopoietic stem cells or most restricted progenitors but depleted common lymphoid progenitors, impairing lymphopoiesis, bacterial clearance, and survival after acute bacterial infection. Peri-arteriolar osteolectin$^+$ cell maintenance required mechanical stimulation. Voluntary running increased, whereas hindlimb unloading decreased, the frequencies of peri-arteriolar osteolectin$^+$ cells and common lymphoid progenitors. Deletion of the mechanosensitive ion channel PIEZO1 from osteolectin$^+$ cells depleted osteolectin$^+$ cells and common lymphoid progenitors. These results show that a peri-arteriolar niche for osteogenesis and lymphopoiesis in bone marrow is maintained by mechanical stimulation and depleted during ageing.

Haematopoietic stem cells (HSCs) and restricted progenitors are maintained in specialized microenvironments, or niches, in haematopoietic tissues in which stromal cells synthesize the growth factors that they require[15]. LEPR$^+$ cells and endothelial cells are the major sources of growth factors for HSC maintenance in adult mouse bone marrow, including SCF[1,3,6], C-X-C motif chemokine 12 (CXCL12)[2,16] and pleiotrophin[5]. LEPR$^+$ cells are also a critical source of SCF and IL-7 for early restricted progenitors, including common lymphoid progenitors (CLPs)[4,6]. The bone marrow environment changes with age[17], contributing to the depletion of lymphoid[18] and osteogenic[19] progenitors. However, beyond changes in the abundance of some types of blood vessel[17,19], little is known about how the environment changes or what causes the depletion of lymphoid and osteogenic progenitors during ageing.

HSCs[20–22] and erythroid progenitors[6] localize adjacent to peri-sinusoidal LEPR$^+$ cells throughout the bone marrow. Single-cell RNA-sequencing (RNA-seq) studies have shown that peri-sinusoidal LEPR$^+$ cells appear poised to undergo adipogenic differentiation, whereas peri-arteriolar LEPR$^+$ cells appear poised to undergo osteogenic differentiation[9–12]. A subset of early lymphoid progenitors resides in an endosteal niche and is maintained by factors from osteoblasts[2,16,23,24]. Other lymphoid progenitors reside in perivascular niches created partly by LEPR$^+$ cells[4,6], although their precise locations remain uncertain.

Oln marks peri-arteriolar LEPR$^+$ cells

To test whether osteolectin expression resolves functionally distinct subsets of LEPR$^+$ cells, we generated *Oln-mTomato* (*Oln^{mT}*) knock-in mice (Extended Data Fig. 1a–c). Flow cytometric analysis of enzymatically dissociated bone marrow cells showed that 0.025 ± 0.007% (all data are mean ± s.d.) of cells were mTomato$^+$ (Fig. 1a). *Oln* transcripts were abundant in mTomato$^+$ cells but were not detected in mTomato$^-$ cells (Extended Data Fig. 1d).

[1]Children's Research Institute and the Department of Pediatrics, University of Texas Southwestern Medical Center, Dallas, TX, USA. [2]Department of Neuroscience, University of Texas Southwestern Medical Center, Dallas, TX, USA. [3]Department of Molecular Biology, University of Texas Southwestern Medical Center, Dallas, TX, USA. [4]Department of Restorative Sciences, School of Dentistry, Texas A&M University, Dallas, TX, USA. [5]School of Biomedical Engineering, Heart Research Institute and Charles Perkins Center, The University of Sydney, Darlington, New South Wales, Australia. [6]Robert J. Tomsich Pathology & Laboratory Medicine Institute, Cleveland Clinic, Cleveland, OH, USA. [7]Howard Hughes Medical Institute, University of Texas Southwestern Medical Center, Dallas, TX, USA. ✉e-mail: Sean.Morrison@UTSouthwestern.edu

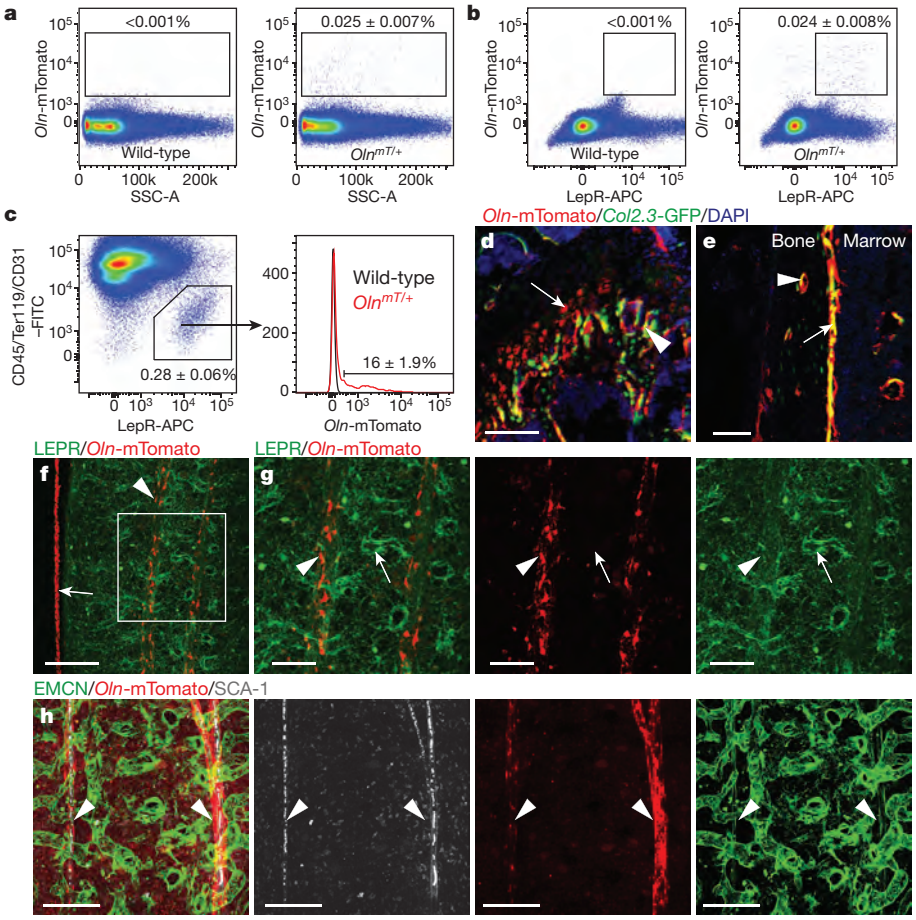

Fig. 1 | Osteolectin is expressed by peri-arteriolar LEPR$^+$ cells. a–**c**, Flow cytometry analysis of enzymatically dissociated bone marrow from *Oln*$^{mT/+}$ mice (four mice per genotype in four independent experiments) **a**, *Oln*-mTomato$^+$ cells represented 0.025% of bone marrow cells. **b**, Most *Oln*-mTomato$^+$ cells were LEPR$^+$. **c**, Only a small minority of LEPR$^+$ cells were *Oln*-mTomato$^+$. **d**, **e**, Representative femur sections showing the epiphysis (**d**) and diaphysis (**e**) from 2-to-4-month-old *Oln*$^{mT/+}$*;Col1a1*2.3*-eGFP mice. **d**, *Oln*-mTomato$^+$ hypertrophic chondrocytes (arrow) and *Oln*-mTomato$^+$*Col1a1*2.3*-eGFP$^+$ osteoblasts in trabecular bone (arrowhead; scale bar, 30 µm). **e**, *Oln*-mTomato$^+$*Col1a1*2.3*-eGFP$^+$ osteoblasts in the endosteum (arrow) and *Oln*-mTomato$^+$ osteocytes (arrowhead; scale bars, 25 µm). **f**, **g**, Deep imaging of *Oln*$^{mT/+}$ femur bone marrow. The boxed area in **f** is magnified in **g**. **f**, Peri-arteriolar *Oln*-mTomato$^+$ cells (arrowhead) and *Oln*-mTomato$^+$ cells on the endosteal surface (arrow; scale bar, 100 µm). **g**, *Oln*-mTomato$^+$LEPR$^+$ peri-arteriolar stromal cells (arrowhead) and *Oln*-mTomato$^-$LEPR$^+$ peri-sinusoidal stromal cells (arrow; scale bar, 40 µm). **h**, *Oln*-mTomato$^+$ cells around SCA-1$^+$ arterioles (arrow) but not Endomucin^{high} sinusoids (scale bar, 200 µm). Images are representative of 3 to 5 experiments with 8-to-10-week-old mice. All data represent mean ± s.d.

Almost all *Oln*-mTomato$^+$ cells in the bone marrow were LEPR$^+$ stromal cells (Fig. 1b), accounting for 16 ± 1.9% of LEPR$^+$ cells (Fig. 1c, Extended Data Fig. 1e, Supplementary Table 1 shows the markers used to identify each cell population). *Oln* transcripts were abundant in *Oln*-mTomato$^+$LEPR$^+$ cells but not detected in *Oln*-mTomato$^-$LEPR$^+$ cells (Extended Data Fig. 1f). We did not detect *Oln*-mTomato in bone marrow endothelial cells (Extended Data Fig. 1g).

Deep confocal imaging[21] of cleared femurs from adult *Oln*^{mT} mice showed that *Oln*-mTomato staining was consistent with antibody staining for osteolectin[13]. In the epiphysis–metaphysis, *Oln*-mTomato was expressed by most hypertrophic chondrocytes and osteoblasts in trabecular bone (Fig. 1d, Extended Data Fig. 1h). In the diaphysis, *Oln*-mTomato was expressed by most osteoblasts and osteocytes in cortical bone (Fig. 1e, Extended Data Fig. 1i) as well as in the periosteum (Extended Data Fig. 1i).

Within the bone marrow, *Oln*-mTomato$^+$ cells were exclusively or nearly exclusively peri-arteriolar. Peri-arteriolar LEPR$^+$ cells were positive for *Oln*-mTomato, whereas peri-sinusoidal LEPR$^+$ cells were negative for *Oln*-mTomato (Fig. 1f, g). Consistently, *Oln*-mTomato$^+$ cells were associated with SCA-1$^+$ arterioles but not endomucin^{high} sinusoids[19,25] (Fig. 1h). These *Oln*-mTomato$^+$ arterioles were mainly in the diaphysis, in the central marrow and near the endosteum (Extended Data Fig. 2a). In the metaphysis, most arterioles were not surrounded by *Oln*-mTomato$^+$ cells (Extended Data Fig. 2b).

We compared the gene expression profiles of CD45$^-$Ter119$^-$CD31$^-$*Scf*-GFP$^+$*Oln*-mTomato$^+$ peri-arteriolar stromal cells and CD45$^-$Ter119$^-$CD31$^-$*Scf*-GFP$^+$*Oln*-mTomato$^-$ peri-sinusoidal stromal cells (both cell populations are uniformly LEPR$^+$). Consistent with single-cell RNA-seq studies[9–12], peri-arteriolar *Oln*-mTomato$^+$ cells were enriched for the expression of osteogenic genes, whereas peri-sinusoidal *Oln*-mTomato$^-$ cells were enriched for adipogenic genes (Extended Data Fig. 2c, d). Both cell populations expressed similar levels of niche (for example, *Scf* and *Cxcl12*) and mesenchymal genes (for example, *Lepr* and *Pdgfrb*) (Supplementary Table 2).

Osteolectin$^+$ cells are osteogenic progenitors

To investigate the function of osteolectin$^+$ cells, we inserted *iCreER* into the *Oln* locus to generate *Oln*^{iCreER} mice (Extended Data Fig. 2e–g). Consistent with the *Oln*-Tomato expression pattern, the *Oln*^{iCreER} allele recombined in peri-arteriolar, but not peri-sinusoidal, stromal cells (Extended Data Fig. 2h) as well as in hypertrophic chondrocytes (Extended Data Fig. 2i), osteoblasts (Extended Data Fig. 2i) and osteocytes (Extended Data Fig. 2j). We found that 91 ± 3.0% and 12 ± 3.3% of fibroblast colony-forming units (CFU-Fs) formed by *Lepr*$^{cre/+}$*;Rosa26*$^{loxp\text{-}tdTomato/+}$ cells and *Oln*$^{iCreER/+}$*;Rosa26*$^{loxp\text{-}tdTomato/+}$ cells, respectively, were tdTomato$^+$ (Fig. 2a). Furthermore, 11 ± 2.4% of *Oln*-mTomato$^-$LEPR$^+$ stromal cells but only 5.2 ± 1.3% of *Oln*-mTomato$^+$LEPR$^+$ cells formed CFU-Fs (Fig. 2b). These data suggest that skeletal stem cells were enriched among osteolectin-negative LEPR$^+$ cells.

When stimulated to differentiate, CFU-Fs formed by *Oln*-mTomato$^+$LEPR$^+$ stromal cells gave rise to significantly more osteoblasts and significantly fewer adipocytes than CFU-Fs formed by *Oln*-mTomato$^-$LEPR$^+$ cells (Fig. 2c, d). When we assessed spontaneous differentiation, the colonies formed by *Oln*-mTomato$^+$LEPR$^+$ cells contained only osteoblasts, whereas colonies formed by *Oln*-mTomato$^-$LEPR$^+$ cells contained osteoblasts and adipocytes (Fig. 2e). *Oln*-mTomato$^+$LEPR$^+$ peri-arteriolar cells were thus enriched for osteogenic progenitors, whereas *Oln*-mTomato$^-$LEPR$^+$ peri-sinusoidal cells were enriched for multipotent cells. *Oln*-mTomato$^+$LEPR$^+$ cells were also more mitotically active (Fig. 2f).

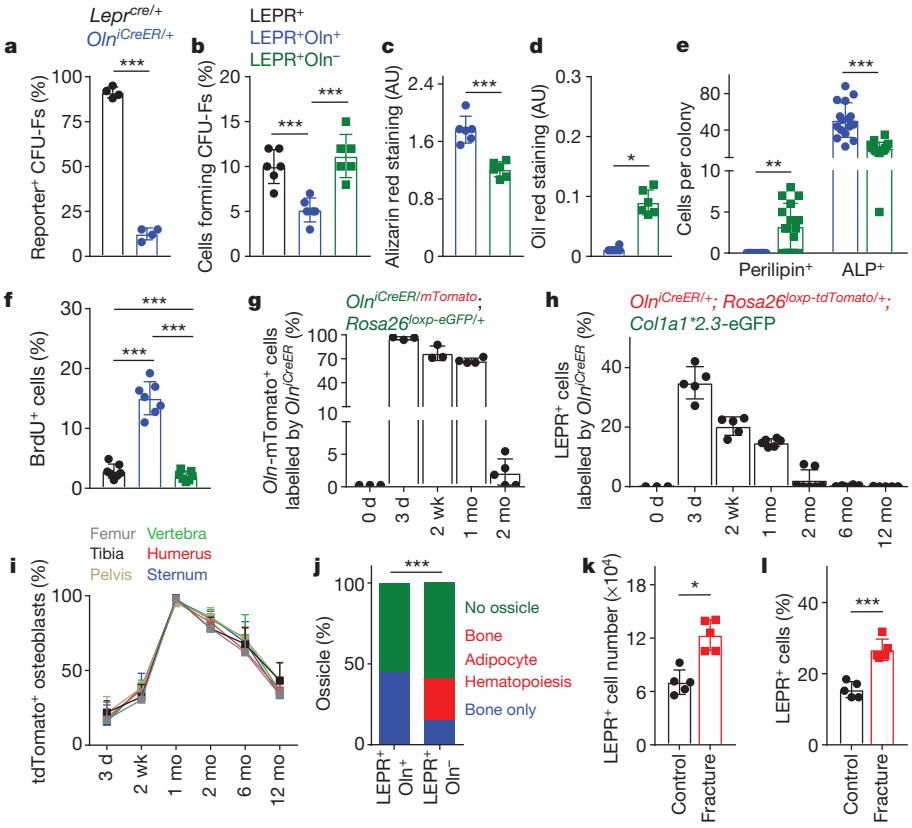

Fig. 2 | Osteolectin$^+$ cells are short-lived osteogenic progenitors. a, Percentage of CFU-F colonies that were tdTomato$^+$ when formed by bone marrow cells from two-month-old *Lepr*$^{cre/+}$;*Rosa26*$^{loxp\text{-}tdTomato/+}$ or *Oln*$^{iCreER/+}$;*Rosa26*$^{loxp\text{-}tdTomato/+}$ mice, three days after tamoxifen administration (four independent experiments). **b**, Percentage of LEPR$^+$, LEPR$^+$*Oln*-mTomato$^+$ and LEPR$^+$*Oln*-mTomato$^-$ bone marrow stromal cells that formed CFU-F colonies. **c**, **d**, Osteogenic (**c**; Alizarin red, $A_{562\,nm}$) and adipogenic (**d**; oil red, $A_{500\,nm}$) differentiation of adherent cells cultured from LEPR$^+$*Oln*-mTomato$^+$ or LEPR$^+$*Oln*-mTomato$^-$ stromal cells (six independent experiments in **b**–**d**). AU, arbitrary units. **e**, The average numbers of perilipin$^+$ adipocytes or alkaline phosphatase$^+$ (ALP$^+$) osteogenic cells that spontaneously differentiated per CFU-F colony after one week of culture (four independent experiments). **f**, Percentage of LEPR$^+$, LEPR$^+$*Oln*-mTomato$^+$ and LEPR$^+$*Oln*-mTomato$^-$ bone marrow stromal cells that incorporated a 24-h pulse of BrdU in vivo (four independent experiments). **g**, Percentage of *Oln*-mTomato$^+$ cells that were eGFP$^+$ in *Oln*$^{iCreER/mT}$;*Rosa26*$^{loxp\text{-}eGFP/+}$ mice treated with tamoxifen at two months of age (three independent experiments). Mo, month; wk, week. **h**, **i**, Percentages of LEPR$^+$ stromal cells (**h**) and *Col1a1*2.3*-eGFP$^+$ osteoblasts (**i**) in tdTomato$^+$*Oln*$^{iCreER/+}$;*Rosa26*$^{loxp\text{-}tdTomato/+}$;*Col1a1*2.3*-eGFP mice treated with tamoxifen at two months of age (five independent experiments). **j**, Bone, adipocytes, and haematopoiesis in ossicles formed by CFU-Fs cultured from LEPR$^+$*Oln*-mTomato$^+$ or LEPR$^+$*Oln*-mTomato$^-$ stromal cells (80 ossicles per cell population derived from 20 mice in 5 independent experiments). **k**, **l**, Femurs were fractured three days after tamoxifen administration to *Oln*$^{iCreER/+}$;*Rosa26*$^{loxp\text{-}tdTomato/+}$;*Col1a1*2.3*-eGFP mice. Two weeks later the number of LEPR$^+$ cells per femur (**k**) and the percentage of LEPR$^+$ cells that were tdTomato$^+$ (**l**) were assessed (five independent experiments). All data represent mean ± s.d. Statistical significance was assessed using an unpaired *t*-test (**a**), paired *t*-tests (**c**, **k**, **l**), matched-samples one-way analysis of variance (ANOVA) followed by Tukey's multiple-comparisons tests (**b**, **f**), Wilcoxon test (**d**), Wilcoxon test followed by Holm–Sidak multiple-comparisons adjustment (**e**), or Cochran–Mantel–Haenszel test (**j**).

In 2-month-old *Oln*$^{mT/iCreER}$;*Rosa26*$^{loxp\text{-}eGFP/+}$ mice, 96 ± 1.8% of *Oln*-mTomato$^+$ cells were eGFP$^+$ 3 days after tamoxifen treatment, indicating high recombination efficiency in peri-arteriolar stromal cells (Fig. 2g). We did not detect eGFP in *Oln*-mTomato$^-$ cells. Two months later, only 1.9 ± 2.2% of *Oln*-mTomato$^+$ cells were eGFP$^+$ (Fig. 2g). Three days after tamoxifen treatment of *Oln*^{iCreER};*Rosa26*$^{loxp\text{-}tdTomato/+}$ mice, 35 ± 5.4% of LEPR$^+$ cells were tdTomato$^+$ (Fig. 2h). These cells were present around arterioles throughout the diaphysis (Extended Data Fig. 2h). However, two months later, only 2.2 ± 3.5% of LEPR$^+$ cells were tdTomato$^+$ (Fig. 2h). Peri-arteriolar *Oln*$^+$ cells are, thus, rapidly dividing and short-lived progenitors.

Oln$^+$ cells are fated to form bone, not fat

We performed lineage tracing in two month-old *Oln*$^{iCreER/+}$;*Rosa26*$^{loxptd\text{-}Tomato/+}$;*Col1a1*2.3*-eGFP mice[26]. Although osteolectin is expressed by osteoblasts (Fig. 1d, e, Extended Data Fig. 2i), only around 20% of *Col1a1*2.3*-eGFP$^+$ bone-lining cells were tdTomato$^+$ in these mice 3 days after tamoxifen treatment, indicating low recombination efficiency in osteoblasts (Fig. 2i). One month after tamoxifen treatment almost all *Col1a1*2.3*-eGFP$^+$ bone-lining cells were tdTomato$^+$, and the percentage continuously declined thereafter (Fig. 2i). Given that endosteal osteoblasts have little proliferative potential[27] and are constantly regenerated from progenitors in the bone marrow[28], this suggests that many new osteoblasts arise from peri-arteriolar *Oln*$^+$ cells, particularly in the diaphysis.

We fate-mapped differentiated osteoblasts by treating two-month-old *Col1a1*-CreER;*Rosa26*$^{loxp\text{-}tdTomato/+}$;*Col1a1*2.3*-eGFP$^+$ mice with tamoxifen. *Col1a1*-CreER does not recombine in LEPR$^+$ stromal cells[1]. tdTomato was expressed by 92 ± 3.2% of *Col1a1*2.3*-eGFP$^+$ osteoblasts 3 days after tamoxifen treatment but by only 24 ± 7.4% of *Col1a1*2.3*-eGFP$^+$ osteoblasts 1 month later (Extended Data Fig. 2k). Endosteal osteoblasts are, therefore, short-lived and constantly regenerated from undifferentiated progenitors.

We sublethally irradiated *Oln*$^{iCreER/+}$;*Rosa26*$^{loxp\text{-}tdTomato/+}$ mice 3 days after tamoxifen treatment and examined the bone marrow 14 days later. We observed large numbers of adipocytes but none were tdTomato$^+$ (Extended Data Fig. 3a).

We also compared the ability of LEPR$^+$*Oln*$^+$ and LEPR$^+$*Oln*$^-$ cells to form bony ossicles in vivo[29]. Thirty-three of 80 denatured collagen sponges

seeded with the progeny of cultured LEPR$^+$*Oln*$^-$ cells formed ossicles after transplantation into immunodeficient NSG mice, 21 of which contained haematopoietic marrow and adipocytes (Fig. 2j, Extended Data Fig. 3b). By contrast, 36 out of 80 sponges seeded with the progeny of cultured LEPR$^+$*Oln*$^+$ cells formed ossicles but none contained haematopoietic marrow or adipocytes (Fig. 2j, Extended Data Fig. 3b). LEPR$^+$*Oln*$^+$ cells are osteogenic progenitors with little skeletal stem cell or adipogenic activity.

We performed femur fractures 3 days after tamoxifen in 2-month-old *Oln*$^{iCreER/+}$;*Rosa26*$^{loxp\text{-}tdTomato/+}$;*Col1a1*2.3*-eGFP$^+$ mice. Two weeks later, we observed a substantial increase in the number of LEPR$^+$ cells and the percentage of LEPR$^+$ cells that were *Oln*-tdTomato$^+$ in the bone marrow (Fig. 2k, l). Within the callus at the fracture site, *Oln*-tdTomato$^+$ cells accounted for 82 ± 10% of *Col1a1*2.3*-eGFP$^+$ osteoblasts. *Oln*$^+$ cells, thus, expand in number after fracture and form most of the osteoblasts that contribute to bone regeneration.

A peri-arteriolar niche for lymphoid progenitors

LEPR$^+$osteolectin$^+$ peri-arteriolar stromal cells and LEPR$^+$osteolectin$^-$ peri-sinusoidal stromal cells were uniformly positive for *Scf*-GFP, with similar levels of expression (Fig. 3a, b). *Scf* deletion from osteolectin$^+$ cells in adult *Oln*$^{iCreER/+}$;*Scf*$^{fl/fl}$ mice did not significantly affect bone marrow or spleen cellularity (Fig. 3c), blood cell counts (Extended Data Fig. 3c–e), or the frequencies of differentiated B-, T-, myeloid-, megakaryocyte- or erythroid-lineage cells in the bone marrow or spleen (Extended Data Fig. 3f–j). Consistent with the localization of HSCs to sinusoidal blood vessels[20–22], *Scf* deletion in peri-arteriolar *Oln*$^+$ cells did not significantly affect HSC or multipotent progenitor (MPP) frequency in the bone marrow (Fig. 3d) or spleen (Extended Data Fig. 3k) or the reconstituting capacity of bone marrow cells in irradiated mice (Extended Data Fig. 3l). *Scf* deletion from *Oln*$^+$ cells also did not significantly affect the frequencies of granulocyte-macrophage progenitors (GMPs), megakaryocyte-erythroid progenitors (MEPs) or common myeloid progenitors (CMPs), but did significantly reduce the frequency of CLPs in the bone marrow (Fig. 3d). The flow cytometry gates used to sort each stem or progenitor cell population are shown in Extended Data Fig. 4.

This suggested that *Oln*$^+$ cells might create a peri-arteriolar niche for CLPs. Although *Oln*^{iCreER} also recombined in a minority of osteoblasts (Fig. 2i), osteoblasts do not express *Scf*[1,9–12] and deletion of *Scf* from osteoblasts does not affect CLP frequency[1]. Consistent with these studies, we did not detect *Scf*-GFP expression in osteolectin$^+$ osteoblasts, osteocytes or hypertrophic chondrocytes (Extended Data Figs. 3m, n, 5a-d). We were unable to find non-peri-arteriolar osteolectin$^+$ cells in the bone marrow that express *Scf*.

Consistent with a peri-arteriolar niche for lymphoid progenitors, 35% of IL7Rα$^+$lineage$^-$ cells (which are mainly CLPs[2]) (Extended Data Fig. 4e) were within 5 μm of peri-arteriolar osteolectin$^+$ cells (Fig. 3e, f; 18-fold more likely than other haematopoietic cells). Consistent with the existence of an endosteal niche for CLPs[2,16,23,24], another 28% of IL7Rα$^+$lineage$^-$ cells were within 5 μm of the endosteal surface (Fig. 3f; sevenfold more likely than other haematopoietic cells). Deletion of *Scf* from osteolectin$^+$ cells significantly reduced the frequency of peri-arteriolar, but not endosteal, IL7Rα$^+$lineage$^-$ cells (Fig. 3g). A subset of early lymphoid progenitors thus resides adjacent to arterioles and depends on SCF from *Oln*$^+$ cells.

To more fully assess the role of this niche in lymphopoiesis, we treated *Oln*$^{iCreER/+}$;*Scf*$^{fl/fl}$ mice and littermate controls with tamoxifen for two months, beginning at two months of age. We did not observe any effect on the frequencies of HSCs, MPPs, GMPs, MEPs or CMPs in the bone marrow (Extended Data Fig. 5e); however, *Oln*$^{iCreER/+}$;*Scf*$^{fl/fl}$ mice did exhibit a broad depletion of lymphoid progenitors including CLPs, pre-pro-B cells and pre-B cells in the bone marrow (Fig. 3h), as well as early thymic progenitors (ETPs) and double negative (DN1 and DN2) thymocytes (Fig. 3i, j). Nonetheless, the numbers of differentiated B and T cells were normal in *Oln*$^{iCreER/+}$;*Scf*$^{fl/fl}$ mice under steady-state conditions (Extended Data Fig. 5f, g).

Fracture did not significantly affect the frequencies of HSCs and MPPs, but did increase the frequencies of *Oln*-mTomato$^+$ cells and CLPs in the bone marrow (Extended Data Fig. 5h, i). Moreover, IL7Rα$^+$lineage$^-$ cells were significantly more likely to be associated with osteolectin$^+$ arterioles in fractured bones compared with control bones (Extended Data Fig. 5j). Conditional deletion of *Scf* from *Oln*$^+$ cells blocked the increase in CLPs after fracture without affecting the frequency of *Oln*-mTomato$^+$ cells (Extended Data Fig. 5h, i).

To test whether increasing bone mass is sufficient to promote the expansion of osteolectin$^+$ cells or CLPs in the bone marrow we administered parathyroid hormone (PTH) to mice daily for a month. PTH treatment significantly increased bone volume (Extended Data Fig. 6a, b) but decreased the frequencies of *Oln*$^+$ stromal cells and CLPs in the bone marrow (Extended Data Fig. 6c, d). Increased bone volume was, therefore, not sufficient to increase *Oln*$^+$ cells and CLPs.

Ageing depletes peri-arteriolar osteolectin$^+$ cells

The frequency of *Oln*-mTomato$^+$ cells in the bone marrow diaphysis declined significantly during ageing (Extended Data Fig. 6e), even though the overall frequency of LEPR$^+$ cells did not change (Extended Data Fig. 6f). In two-month-old mice, nearly all arterioles in the diaphysis were surrounded by osteolectin$^+$ cells (Figs. 1h, 3a). In 18-month-old mice, about half of peri-arteriolar regions in the diaphysis lacked osteolectin$^+$ cells in the central marrow and near the endosteum (Extended Data Fig. 6g). CLPs were also depleted during ageing (Extended Data Fig. 6h). By contrast, frequencies of HSC and MPP increased during ageing[18,30] and those of GMPs, CMPs and MEPs did not change (Extended Data Fig. 6i–m). The percentage of IL7Rα$^+$lineage$^-$ cells associated with arterioles declined during ageing (Extended Data Fig. 6n), particularly around arterioles that lacked osteolectin$^+$ cells (Extended Data Fig. 6o, p). This suggests that the age-related decline in lymphoid progenitors may be caused partly by the loss of osteolectin$^+$ cells.

Peri-arteriolar niches promote infection response

We tested whether the peri-arteriolar niche was necessary for lymphopoiesis after acute infection with a bacterium the clearance of which depends upon T and B cells[31,32]. Three days after tamoxifen treatment, *Oln*$^{iCreER/+}$;*Scf*$^{fl/fl}$ mice and littermate controls were administered *Listeria monocytogenes* by oral gavage. In the absence of *Listeria*, B and T cell counts were similar in *Oln*$^{iCreER/+}$;*Scf*$^{fl/fl}$ mice and littermate controls (Extended Data Fig. 7a, b). After *Listeria* infection, B and T cell counts significantly increased in the spleens of control, but not *Oln*$^{iCreER/+}$;*Scf*$^{fl/fl}$, mice and bacterial counts were significantly increased in the spleens of *Oln*$^{iCreER/+}$;*Scf*$^{fl/fl}$ mice compared with those of control mice (Extended Data Fig. 7a–c). Osteolectin$^+$ peri-arteriolar niches thus appeared to be required to augment lymphopoiesis and to clear bacteria after acute infection.

We also administered *Listeria* intraperitoneally. Relative to controls, *Oln*$^{iCreER/+}$;*Scf*$^{fl/fl}$ mice had fewer CLPs (Fig. 3k) and pre-proB cells in the bone marrow (Extended Data Fig. 7d), as well as fewer ETPs and DN1 cells in the thymus (Extended Data Fig. 7e) at 5 and 10 days after infection. We also observed reduced numbers of B, T and NK1.1$^+$CD3$^-$ natural killer (NK) cells (Extended Data Fig. 7f–i, l, m), impaired *Listeria* clearance (Extended Data Fig. 7j, n) and reduced survival (Fig. 3l). We observed no change in IFNγ levels in T cells from *Oln*$^{iCreER/+}$;*Scf*$^{fl/fl}$ mice compared with those from control mice (Extended Data Fig. 7k), suggesting normal T cell activation. The peri-arteriolar niche is thus required for the maintenance of normal numbers of lymphoid progenitors and lymphocytes during the response to acute bacterial infection.

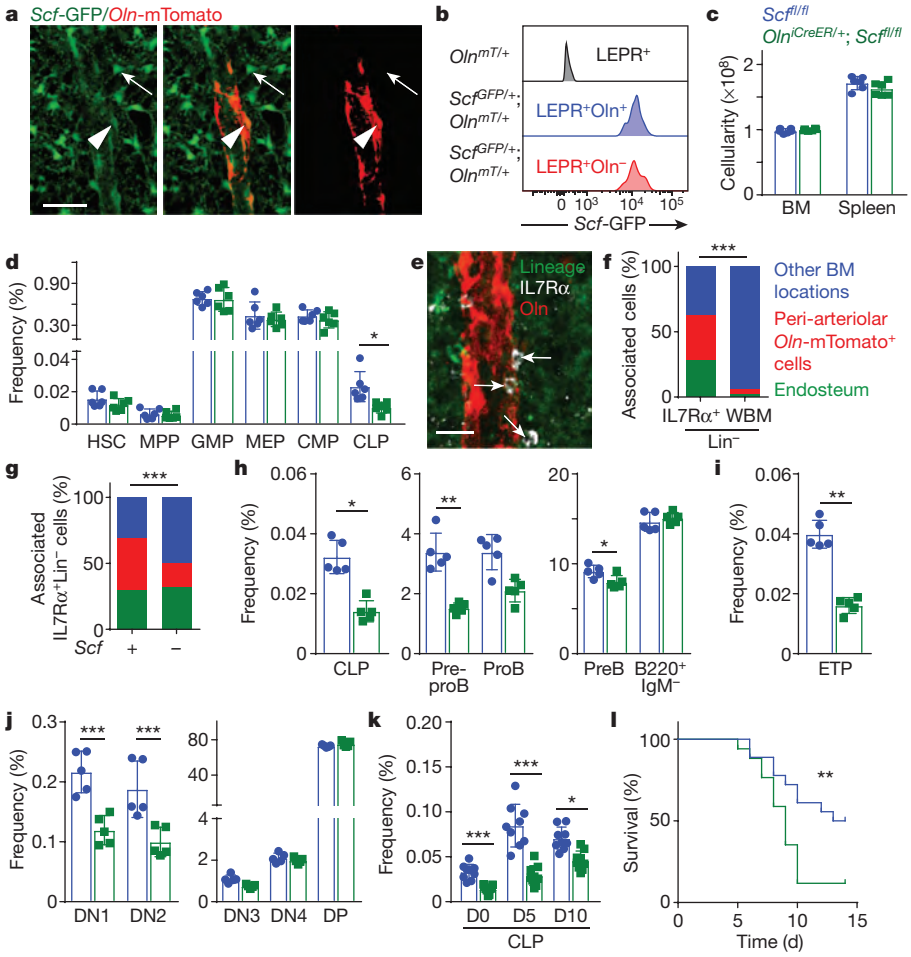

Fig. 3 | Osteolectin$^+$ peri-arteriolar stromal cells maintain early lymphoid progenitors by synthesizing SCF. a, **b**, In femur bone marrow from 2-month-old *Scf*$^{GFP/+}$;*Oln*$^{mT/+}$ mice, *Scf*-GFP was expressed by both *Oln*-mTomato$^+$ peri-arteriolar cells (arrowhead in **a**) and *Oln*-mTomato$^-$ peri-sinusoidal cells (arrow in **a**; scale bar, 20 μm), at comparable levels (**b**). **c**, **d**, *Oln*$^{iCreER/+}$;*Scf*$^{fl/fl}$ and *Scf*$^{fl/fl}$ littermate control mice were treated with tamoxifen at two months of age; bone marrow (BM) and spleen cellularity (**c**), and haematopoietic stem and progenitor cell frequencies in the bone marrow (**d**) were analysed one month later (three independent experiments). **e**, **f**, Localization (**e**) and quantification (**f**) of IL7Rα$^+$lineage$^-$ lymphoid progenitors (arrows) adjacent to peri-arteriolar osteolectin$^+$ (Oln) cells (scale bar, 15 μm; nine mice in three independent experiments). WBM, whole bone marrow. **g**, Localization of IL7Rα$^+$lineage$^-$ cells in the bone marrow of *Oln*$^{iCreER/+}$;*Scf*$^{fl/fl}$ and *Scf*$^{fl/fl}$ littermate control mice (six mice per genotype in three independent experiments). **h**–**j**, *Oln*$^{iCreER/+}$;*Scf*$^{fl/fl}$ mice and littermate controls were fed tamoxifen from two to four months of age and the bone marrow (**h**) and thymus (**i**, **j**) were analysed (three independent experiments). **k**, **l**, Compared to *Scf*$^{fl/fl}$ controls, *Oln*$^{iCreER/+}$;*Scf*$^{fl/fl}$ mice had decreased CLP frequency in the bone marrow (**k**) and worse survival (**l**) after *Listeria* infection (17–27 mice per genotype in 3 independent experiments). Images are representative of three independent experiments. The same differences that were evident among the frequencies of cell populations were also evident in absolute numbers. All data represent mean ± s.d. Statistical significance was assessed using matched-samples two-way ANOVA followed by Sidak's multiple-comparisons tests (**c**, **d**, **h**–**k**), Cochran–Mantel–Haenszel tests (**f**, **g**), or Mantel–Cox test (**l**).

Mechanosensation maintains peri-arteriolar niches

To test whether exercise could restore peri-arteriolar niches in ageing bone marrow, running wheels were placed in the cages of 18-month-old *Oln*$^{mT/+}$ mice for 4 weeks. Voluntary running increased bone mineral density (Extended Data Fig. 8a) and cortical bone thickness (Fig. 4a), as well as the frequencies of *Oln*-mTomato$^+$ cells (Fig. 4b) and CLPs (Fig. 4c) relative to non-running control mice. Voluntary running did not significantly affect the frequencies of HSCs, MPPs, GMPs, MEPs or CMPs (Fig. 4c). Voluntary running increased CLP frequency in load-bearing long bones (Fig. 4c) but not in the calvarium of the same mice (Extended Data Fig. 8b). Voluntary running thus appeared to promote the expansion of peri-arteriolar niches in load-bearing bones.

To test whether mechanical loading is required for osteolectin$^+$ cell maintenance, we suspended the hindlimbs of two-month-old *Oln*$^{mT/+}$ mice for two weeks to reduce mechanical loading on the hindlimbs while they walked on their forelimbs[33] (Extended Data Fig. 8c). In the forelimbs, we observed no significant effects on bone mineral density, cortical bone thickness or the frequencies of *Oln*-mTomato$^+$ cells, CLPs, HSCs, MPPs, GMPs, MEPs or CMPs in the bone marrow (Extended Data Fig. 8d–g). By contrast, the femurs of suspended mice exhibited significantly reduced bone mineral density (Extended Data Fig. 8h), cortical bone thickness, *Oln*-mTomato$^+$ cell frequency and CLP frequency relative to control mice (Fig. 4d–f). The depletion of osteolectin$^+$ cells after unloading may have been caused by reduced proliferation as we observed reduced BrdU incorporation (Fig. 4g). We did not detect any effect of hindlimb suspension on the frequencies of HSCs, MPPs, GMPs, MEPs or CMPs (Fig. 4f). Hindlimb unloading thus reduced the frequencies of *Oln*-mTomato$^+$ cells and CLPs, suggesting that mechanical loading is required for the maintenance of peri-arteriolar niches.

Gene-expression profiling and western blotting showed that osteolectin$^+$ cells express the stretch-induced ion channel PIEZO1[34,35] (Fig. 4k). Mechanical loading promotes bone formation and increases skeletal bone mass[36], partly by promoting PIEZO1 signalling in mesenchymal progenitors during development[37] and in osteoblasts during adulthood[34,35,38]. To test whether mechanical stimulation

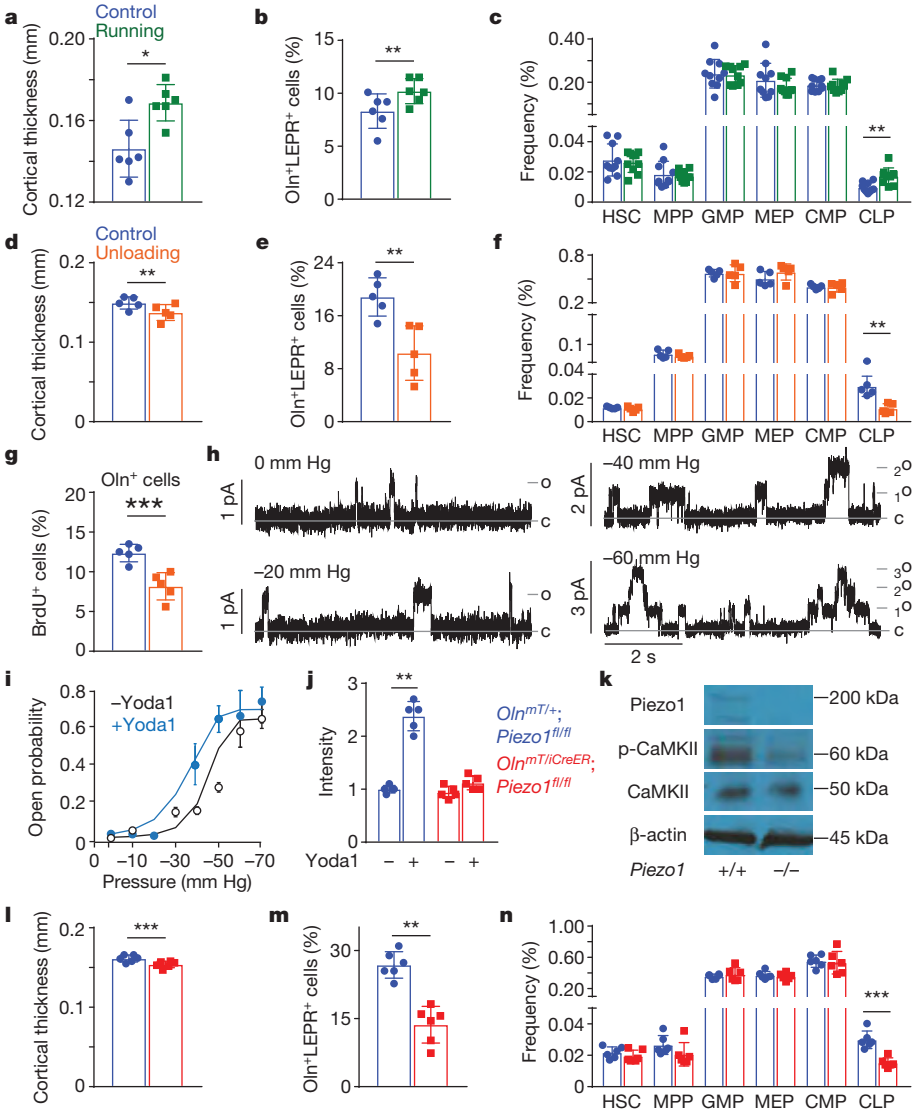

Fig. 4 | Mechanical stimulation is required for the maintenance of peri-arteriolar niches for lymphoid progenitors in the bone marrow. **a**–**c**, The effect of voluntary running for 4 weeks on femoral cortical thickness (**a**), the percentage of LEPR$^+$ cells that were *Oln*-mTomato$^+$ (**b**) and the frequencies of haematopoietic stem and progenitor cells in the bone marrow (**c**) (6–10 mice per treatment in 3–5 independent experiments). **d**–**g**, The effect of hindlimb unloading for 2 weeks on femur cortical thickness (**d**), the percentage of LEPR$^+$ cells that were *Oln*-mTomato$^+$ (**e**), the frequencies of stem and progenitors cells in the bone marrow (**f**), and the percentage of osteolectin$^+$ cells that incorporated a 48-h pulse of BrdU (**g**) (5 mice per treatment in 3 independent experiments). **h**, Single-channel current recordings in *Oln*-mTomato$^+$ cells at the indicated applied pressures. O and C denote the open and closed states of the channels, respectively. **i**, Normalized open probability–pressure relationship from *Oln*-mTomato$^+$ cells recorded with (blue) or without (white) 40 μM Yoda1 in the patch pipette (6 mice in 6 independent experiments). **j**, Yoda1-mediated Ca^{2+} response in *Oln*-mTomato$^+$ cells isolated from *Oln*$^{mT/iCreER}$;*Piezo1*$^{fl/fl}$ or *Oln*$^{mT/+}$;*Piezo1*$^{fl/fl}$ littermate control mice (5 mice per genotype in 3 independent experiments). **k**, Western blot of osteolectin$^+$ cells from *Oln*$^{mT/iCreER}$;*Piezo1*$^{fl/fl}$ or *Oln*$^{mT/+}$;*Piezo1*$^{fl/fl}$ mice (representative of three independent experiments). **l**–**n**, The effect of *Piezo1* deletion in osteolectin$^+$ cells on cortical thickness (**l**), the percentage of LEPR$^+$ cells that were *Oln*-mTomato$^+$ (**m**) and the frequencies of stem and progenitor cells in bone marrow (**n**) (6 mice per genotype in 3 independent experiments). The same differences that were evident among the frequencies of cell populations were also evident in absolute numbers. All data represent mean ± s.d. Statistical significance was assessed using paired *t*-tests (**a**, **b**, **g**, **l**, **m**) and matched-samples two-way ANOVAs followed by Sidak's (**c**–**e**, **j**, **n**) or Holm–Sidak (**f**) multiple-comparisons adjustments.

elicits piezo-like channel activity in osteolectin$^+$ cells, we sorted LEPR$^+$osteolectin$^+$ cells into culture and performed patch clamp recordings with negative applied pressures[37,39] (Fig. 4h, Extended Data Fig. 8i). We observed piezo-like channel properties in osteolectin$^+$ cells that recapitulated previously reported PIEZO1 single channel conductance and pressure-dependent activity[37]. The channels were sensitized by Yoda1, a pharmacological agonist of PIEZO1[40]. The calculated $P_{1/2}$ (pressure at which half of the channels are open) was −35 mm Hg with Yoda1 and −45 mm Hg in the absence of Yoda1 (Fig. 4i). Pressure-dependent and Yoda1-dependent channel activity were not observed in osteolectin$^+$ cells from *Oln*$^{mT/iCreER}$;*Piezo1*$^{fl/fl}$ mice (Extended Data Fig. 8j, k). A Yoda1-induced calcium influx was observed in osteolectin$^+$ cells from control, but not *Oln*$^{mT/iCreER}$;*Piezo1*$^{fl/fl}$ mice (Fig. 4j).

Piezo1 deletion from *Oln*$^+$ cells at two months of age significantly reduced *Piezo1* transcript and protein levels in osteolectin$^+$ cells (Fig. 4k, Extended Data Fig. 8l) as well as bone mineral density (Extended Data Fig. 8m), cortical bone thickness (Fig. 4l), *Oln*-mTomato$^+$ cell frequency (Fig. 4m) and CLP frequency (Fig. 4n). The depletion of osteolectin$^+$ cells after *Piezo1* deletion may have been caused by reduced proliferation as we observed reduced BrdU incorporation (Extended Data Fig. 8n). The percentage of CLPs associated with arterioles also significantly declined after *Piezo1* deletion (Extended Data Fig. 8o). We did not detect

any effect of *Piezo1* deletion on the frequencies of HSCs, MPPs, GMPs, MEPs or CMPs (Fig. 4n). The phosphorylation of calcium/calmodulin-dependent protein kinase II (CaMKII), a downstream mediator of piezo signalling, was reduced in *Piezo1*-deficient compared with control osteolectin$^+$ cells (Fig. 4k). PIEZO1 thus acts in osteolectin$^+$ cells to maintain a peri-arteriolar niche for osteogenic and lymphoid progenitors.

We conditionally deleted *Piezo1* in osteoblasts using *Col1a1*-CreER and in all LEPR$^+$ cells using *Lepr^{cre}*. *Col1a1*-CreER*;Piezo1$^{fl/fl}$;Oln$^{mT/+}$* mice had reduced bone mass as compared to sex-matched littermate controls (Extended Data Fig. 8p, q), consistent with PIEZO1 function in osteoblasts[34,35,38]. However, there were no differences between *Col1a1*-CreER*;Piezo1$^{fl/fl}$;Oln$^{mT/+}$* and control mice in the frequencies of osteolectin$^+$LEPR$^+$ bone marrow cells (Extended Data Fig. 8r) or haematopoietic stem or progenitor cells (Extended Data Fig. 8s). Therefore, the maintenance of peri-arteriolar osteolectin$^+$ cells and CLPs does not require mechanical stimulation of osteoblasts.

We also examined *Lepr$^{cre/+}$;Piezo1$^{fl/fl}$;Oln$^{mT/+}$* mice, in which *Piezo1* was deleted from both peri-arteriolar LEPR$^+$osteolectin$^+$ cells and peri-sinusoidal LEPR$^+$osteolectin$^-$ cells. The bone mass and CLP depletion phenotypes were not more severe in *Lepr$^{cre/+}$;Piezo1$^{fl/fl}$;Oln$^{mT/+}$* mice (Extended Data Fig. 8t–w) compared with *Oln$^{mT/iCreER}$;Piezo1$^{fl/fl}$* mice (Fig. 4l–n). Moreover, *Piezo1* deletion from all LEPR$^+$ cells had no effect on the frequencies of HSCs, MPPs, GMPs, MEPs or CMPs (Extended Data Fig. 8w). This suggests that mechanical stimulation is not required for the maintenance of peri-sinusoidal niches. Mechanical forces may selectively regulate the maintenance of peri-arteriolar niches.

Finally, we tested whether mechanosensation in osteolectin$^+$ cells promoted the response to acute infection. Three days after tamoxifen treatment, *Oln$^{mT/iCreER}$;Piezo1$^{fl/fl}$* mice and littermate controls were administered oral *Listeria*. In the absence of *Listeria*, B and T cell counts were similar in the spleens of *Oln$^{mT/iCreER}$;Piezo1$^{fl/fl}$* and control mice (Extended Data Fig. 8x, y). After *Listeria* infection, numbers of B and T cells were significantly reduced and bacterial counts were significantly increased in the spleens of *Oln$^{mT/iCreER}$;Piezo1$^{fl/fl}$* compared with those of control mice (Extended Data Fig. 8x–z). Loss of PIEZO1 from osteolectin$^+$ cells thus, impaired lymphopoiesis and bacterial clearance after acute infection.

Arteriolar endothelial cells may also regulate the maintenance of lymphoid progenitors in peri-arteriolar niches, as deletion of Notch ligand from arteriolar endothelial cells impairs lymphopoiesis[9]. Arterioles may be particularly effective at transmitting movement-induced mechanical stimuli from the bone into the marrow because they are thicker and stiffer walled than sinusoids[41] and often enter the bone marrow by passing through cortical bone[42,43]. Mammalian stem–progenitor cell niches thus sometimes require mechanical stimulation for their maintenance.

Online content

Any methods, additional references, Nature Research reporting summaries, source data, extended data, supplementary information, acknowledgements, peer review information; details of author contributions and competing interests; and statements of data and code availability are available at https://doi.org/10.1038/s41586-021-03298-5.

1. Ding, L., Saunders, T. L., Enikolopov, G. & Morrison, S. J. Endothelial and perivascular cells maintain haematopoietic stem cells. *Nature* **481**, 457–462 (2012).
2. Ding, L. & Morrison, S. J. Haematopoietic stem cells and early lymphoid progenitors occupy distinct bone marrow niches. *Nature* **495**, 231–235 (2013).
3. Oguro, H., Ding, L. & Morrison, S. J. SLAM family markers resolve functionally distinct subpopulations of hematopoietic stem cells and multipotent progenitors. *Cell Stem Cell* **13**, 102–116 (2013).
4. Cordeiro Gomes, A. et al. Hematopoietic stem cell niches produce lineage-instructive signals to control multipotent progenitor differentiation. *Immunity* **45**, 1219–1231 (2016).
5. Himburg, H. A. et al. Distinct bone marrow sources of pleiotrophin control hematopoietic stem cell maintenance and regeneration. *Cell Stem Cell* **23**, 370–381 (2018).
6. Comazzetto, S. et al. Restricted hematopoietic progenitors and erythropoiesis require SCF from leptin receptor$^+$ niche cells in the bone marrow. *Cell Stem Cell* **24**, 477–486 (2019).
7. Zhou, B. O., Yue, R., Murphy, M. M., Peyer, J. G. & Morrison, S. J. Leptin-receptor-expressing mesenchymal stromal cells represent the main source of bone formed by adult bone marrow. *Cell Stem Cell* **15**, 154–168 (2014).
8. Zhou, B. O. et al. Bone marrow adipocytes promote the regeneration of stem cells and haematopoiesis by secreting SCF. *Nat. Cell Biol.* **19**, 891–903 (2017).
9. Tikhonova, A. N. et al. The bone marrow microenvironment at single-cell resolution. *Nature* **569**, 222–228 (2019).
10. Baryawno, N. et al. A cellular taxonomy of the bone marrow stroma in homeostasis and leukemia. *Cell* **177**, 1915–1932 (2019).
11. Baccin, C. et al. Combined single-cell and spatial transcriptomics reveal the molecular, cellular and spatial bone marrow niche organization. *Nat. Cell Biol.* **22**, 38–48 (2020).
12. Matsushita, Y. et al. A Wnt-mediated transformation of the bone marrow stromal cell identity orchestrates skeletal regeneration. *Nat. Commun.* **11**, 332 (2020).
13. Yue, R., Shen, B. & Morrison, S. J. Clec11a/osteolectin is an osteogenic growth factor that promotes the maintenance of the adult skeleton. *eLife* **5**, e18782 (2016).
14. Shen, B. et al. Integrin alpha11 is an Osteolectin receptor and is required for the maintenance of adult skeletal bone mass. *eLife* **8**, e42274 (2019).
15. Crane, G. M., Jeffery, E. & Morrison, S. J. Adult haematopoietic stem cell niches. *Nat. Rev. Immunol.* **17**, 573–590 (2017).
16. Greenbaum, A. et al. CXCL12 in early mesenchymal progenitors is required for haematopoietic stem-cell maintenance. *Nature* **495**, 227–230 (2013).
17. Saçma, M. et al. Haematopoietic stem cells in perisinusoidal niches are protected from ageing. *Nat. Cell Biol.* **21**, 1309–1320 (2019).
18. Young, K. et al. Progressive alterations in multipotent hematopoietic progenitors underlie lymphoid cell loss in aging. *J. Exp. Med.* **213**, 2259–2267 (2016).
19. Kusumbe, A. P. et al. Age-dependent modulation of vascular niches for haematopoietic stem cells. *Nature* **532**, 380–384 (2016).
20. Kiel, M. J. et al. SLAM family receptors distinguish hematopoietic stem and progenitor cells and reveal endothelial niches for stem cells. *Cell* **121**, 1109–1121 (2005).
21. Acar, M. et al. Deep imaging of bone marrow shows non-dividing stem cells are mainly perisinusoidal. *Nature* **526**, 126–130 (2015).
22. Christodoulou, C. et al. Live-animal imaging of native haematopoietic stem and progenitor cells. *Nature* **578**, 278–283 (2020).
23. Visnjic, D. et al. Hematopoiesis is severely altered in mice with an induced osteoblast deficiency. *Blood* **103**, 3258–3264 (2004).
24. Zhu, J. et al. Osteoblasts support B-lymphocyte commitment and differentiation from hematopoietic stem cells. *Blood* **109**, 3706–3712 (2007).
25. Kusumbe, A. P., Ramasamy, S. K. & Adams, R. H. Coupling of angiogenesis and osteogenesis by a specific vessel subtype in bone. *Nature* **507**, 323–328 (2014).
26. Kalajzic, Z. et al. Directing the expression of a green fluorescent protein transgene in differentiated osteoblasts: comparison between rat type I collagen and rat osteocalcin promoters. *Bone* **31**, 654–660 (2002).
27. Dobnig, H. & Turner, R. T. Evidence that intermittent treatment with parathyroid hormone increases bone formation in adult rats by activation of bone lining cells. *Endocrinology* **136**, 3632–3638 (1995).
28. Park, D. et al. Endogenous bone marrow MSCs are dynamic, fate-restricted participants in bone maintenance and regeneration. *Cell Stem Cell* **10**, 259–272 (2012).
29. Bianco, P., Kuznetsov, S. A., Riminucci, M. & Gehron Robey, P. Postnatal skeletal stem cells. *Methods Enzymol.* **419**, 117–148 (2006).
30. Morrison, S. J., Wandycz, A. M., Akashi, K., Globerson, A. & Weissman, I. L. The aging of hematopoietic stem cells. *Nat. Med.* **2**, 1011–1016 (1996).
31. Ladel, C. H., Flesch, I. E., Arnoldi, J. & Kaufmann, S. H. Studies with MHC-deficient knock-out mice reveal impact of both MHC I- and MHC II-dependent T cell responses on Listeria monocytogenes infection. *J. Immunol.* **153**, 3116–3122 (1994).
32. Kayraklioglu, N., Horuluoglu, B., Elango, M. & Klinman, D. M. Critical role of B cells in Toll-like receptor 7-mediated protection against *Listeria monocytogenes* infection. *Infect. Immun.* **87**, e00742-19 (2019).
33. Robling, A. G. et al. Mechanical stimulation of bone in vivo reduces osteocyte expression of Sost/sclerostin. *J. Biol. Chem.* **283**, 5866–5875 (2008).
34. Li, X. et al. Stimulation of Piezo1 by mechanical signals promotes bone anabolism. *eLife* **8**, e49631 (2019).
35. Sun, W. et al. The mechanosensitive Piezo1 channel is required for bone formation. *eLife* **8**, e47454 (2019).
36. Iwaniec, U. T. & Turner, R. T. Influence of body weight on bone mass, architecture and turnover. *J. Endocrinol.* **230**, R115–R130 (2016).
37. Coste, B. et al. Piezo1 and Piezo2 are essential components of distinct mechanically activated cation channels. *Science* **330**, 55–60 (2010).
38. Wang, L. et al. Mechanical sensing protein PIEZO1 regulates bone homeostasis via osteoblast-osteoclast crosstalk. *Nat. Commun.* **11**, 282 (2020).
39. Coste, B. et al. Piezo proteins are pore-forming subunits of mechanically activated channels. *Nature* **483**, 176–181 (2012).
40. Syeda, R. et al. Chemical activation of the mechanotransduction channel Piezo1. *eLife* **4**, e07369 (2015).
41. Boron, W. F. & Boulpaep, E. L. *Medical Physiology* 2nd edn. Ch. 19 (Saunders, 2009).
42. Grüneboom, A. et al. A network of trans-cortical capillaries as mainstay for blood circulation in long bones. *Nat. Metab.* **1**, 236–250 (2019).
43. Sivaraj, K. K. & Adams, R. H. Blood vessel formation and function in bone. *Development* **143**, 2706–2715 (2016).

Methods

No statistical methods were used to predetermine sample size. The experiments were not randomized except that mice were randomly assigned to treatments. The investigators were generally not blinded to allocation during experiments and outcome assessment, except for *Listeria* infection experiments in which data were collected in a manner blinded to sample identity.

Mice

All mouse experiments complied with all relevant ethical regulations and were performed according to protocols approved by the Institutional Animal Care and Use Committees at University of Texas Southwestern Medical Center (protocol 2017-101896) and Texas A&M Health Science Center (2018-0217-CD). All mice were maintained on a C57BL/Ka background, including *Lepr*^{cre} (ref. [44]), *Rosa26-CAG-loxp-stop-loxp-tdTomato* (Ai14)[45], *Rosa26-CAG-loxp-stop-loxp-eGFP* (Ai47)[46], *Col1a1*2.3*-eGFP[26], *Piezo1*^{flox} (ref. [47]), *Scf*^{flox} and *Scf*^{GFP} (ref. [1]) mice. To generate *Oln*^{mT} and *Oln*^{iCreER} mice, CleanCap Cas9 mRNA (TriLink) and sgRNAs (transcribed using MEGAshortscript Kit (Ambion) and purified using the MEGAclear Kit (Ambion)), and recombineering plasmids were microinjected into C57BL/Ka zygotes. Chimeric mice were genotyped by restriction fragment length polymorphism analysis and insertion of the mTomato sequence[48] into the correct locus was confirmed by Southern blotting and sequencing of the targeted allele. Founders were mated with C57BL/Ka mice to obtain germline transmission then backcrossed with wild-type C57BL/Ka mice for at least three generations before analysis. To induce Cre recombinase activity, unless otherwise indicated, *Oln*$^{iCreER/+}$ mice received a daily intraperitoneal injection of 1 mg of tamoxifen dissolved in corn oil for 5 days. All mice were housed in specific pathogen-free animal care facilities under a 12 h:12 h light:dark cycle with a temperature of 18–24 °C and humidity of 35–60%.

Genotyping primers

Primers for genotyping *Oln*^{mT} mice were 5′-TCT GGG AGA CCA CAG AGA CTC AAGG, 5′- AAA GAC AGA AGG CAC AAC TAG AGGC, 5′-CAA TTC CGT GGT GTT GTC GGG GAA ATC ATC, and 5′-CAC TGT GAA AAG ACA GAA GGC ACA ACT AGAG. Primers for genotyping *Oln*^{iCreER} mice were 5′-TCA AGA GTT TAA CCC ACT GAA CTT CAT AGA, 5′-CTC GTT AGA GCA GTA GTG TGT TAG TGAA, 5′-TGG GTA GAC CCA AGG CGG GA, and 5′-GGA GGG CAG GCA GGT TTT GGT.

Flow cytometry

Bone marrow haematopoietic cells were isolated by flushing the long bones with Ca^{2+}- and Mg^{2+}-free HBSS (HBSS-free) with 2% heat-inactivated bovine serum. Spleen cells were obtained by crushing the spleen between two glass slides. The cells were dissociated into a single cell suspension by gently passing them through a 25-gauge needle and then filtering through 70-µm nylon mesh. HSCs were isolated using anti-CD150 (TC15-12F12.2), anti-CD48 (HM48-1), anti-SCA1 (E13-161.7), and anti-KIT (2B8) along with the following antibodies against lineage markers: anti-Ter119, anti-B220 (6B2), anti-Gr1 (8C5), anti-CD2 (RM2-5), anti-CD3 (17A2), anti-CD5 (53-7.3) and anti-CD8 (53-6.7). Haematopoietic progenitors were isolated with the lineage markers anti-Ter119, anti-B220, anti-Gr1, anti-CD2, anti-CD3, anti-CD5, and anti-CD8 as well as additional antibodies against CD34 (RAM34), CD135 (FLT3) (A2F10), CD16/32 (FcγR) (clone 93), CD127 (IL7Ra) (A7R34), CD43 (1B11), CD24 (M1/69), IgM (II/41), CD44 (IM7), and CD25 (PC61.5). DAPI was used to exclude dead cells. The markers used to identify each cell population in this study are summarized in Supplementary Table 1. All antibodies were used at 1:200 dilution unless otherwise specified.

For flow cytometry analysis of stromal cells, bone marrow was flushed using HBSS-free with 2% bovine serum. Then whole bone marrow was digested with type I collagenase (3 mg ml^{-1}), dispase (4 mg ml^{-1}) and DNase I (1 U ml^{-1}) at 37 °C for 30 min as previously described[14]. Samples were then stained with antibodies and analysed by flow cytometry. Goat-anti-LEPR-biotin (AF497), anti-CD45 (30F-11), anti-CD31 (clone 390) and anti-TER119 antibodies were used to isolate LEPR^{+} cells. For analysis of bone marrow endothelial cells, mice were intravenously injected with 10 µg per mouse of eFluor660-conjugated anti-VE-cadherin antibody (BV13, eBiosciences). Ten minutes later, the long bones were removed and bone marrow was flushed, digested and stained as above. Samples were analysed using FACSAria or FACSCanto II flow cytometers and FACSDiva 8.0 (BD) or FlowJo v.10.6.1 (Tree Star) software.

Immunostaining of bone sections

Freshly dissected mouse femurs were fixed in 4% paraformaldehyde overnight. Bones were decalcified in phosphate-buffered saline (PBS) with 10% EDTA and 30% sucrose for 5 days. Bones were sectioned in 12-µm slices using the CryoJane tape-transfer system (Leica). Sections were blocked in PBS with 5% normal donkey serum (Jackson Immuno) for 1 h and then stained overnight with chicken-anti-GFP (Aves), rabbit-anti-tomato (Takara), and goat-anti-LEPR-biotin (R&D Systems). Donkey anti-chicken Alexa Fluor 488 (Jackson Immuno), donkey anti-goat Alexa Fluor 488 (Jackson Immuno), donkey anti-goat Alexa Fluor 555 (Invitrogen) and donkey anti-rabbit Alexa Fluor 647 (Jackson Immuno) were used as secondary antibodies. Slides were mounted with Prolong Gold anti-fade medium (Invitrogen). To identify CLPs, mice were intravenously injected with 2 µg Alexa Fluor 647 anti-IL7Rα (A7R34, Biolegend). After 5 min, the mice were killed and long bones were dissected, fixed, sectioned and stained with antibodies against lineage markers (anti-CD2, CD3, CD5, CD8, TER119, GR1 and B220). Images were acquired with a Zeiss LSM780 or a Leica SP8 confocal microscope. Confocal images were processed and analysed using Zeiss Zen-2 or Leica LAS X.

Deep imaging of half bones

Femurs were longitudinally cut in half, then stained and deep imaged as previously described[21]. The staining solution contained 10% DMSO, 0.5% IgePal630 (Sigma) and 5% donkey serum (Jackson Immuno) in PBS. Half bones were stained for 3 days at room temperature with primary antibodies. Then specimens were washed 3 times in PBS at room temperature for 1 day and put into staining solution containing secondary antibodies for 3 days followed by a 1 day wash. Antibodies used for whole mount staining included chicken anti-GFP (Aves Labs, 1:200), anti-tdTomato (Takara, 1:200), Alexa Fluor 647-AffiniPure F(ab′)2 Fragment Donkey Anti-Chicken IgY (1:250), Alexa Fluor 488-AffiniPure F(ab′)2 Fragment Donkey Anti-Rabbit IgG (1:250), Alexa Fluor 488-AffiniPure F(ab′)2 Fragment Donkey Anti-Rabbit IgG (all from Jackson ImmunoResearch, 1:250), and 555–conjugated donkey anti-goat antibody (Invitrogen, 1:250). Images were acquired using a Leica SP8 confocal microscope. Images were rendered in 3D and analysed using Bitplane Imaris v.7.7.1.

CFU-F and in vitro differentiation assay

Freshly dissociated bone marrow cells were plated at clonal density in 6-well plates pre-coated with 100 ng ml^{-1} fibronectin (Sigma) overnight. The cells were cultured in DMEM-low glucose (Gibco) plus 20% fetal bovine serum (Sigma), 10 mM ROCK inhibitor Y-27632 (Selleck) and 1% penicillin/streptomycin (Invitrogen) at 37 °C in gas-tight chambers (Billups-Rothenberg) flushed with 1% O_2 and 6% CO_2 (balance Nitrogen) to maintain physiological oxygen levels that promoted survival and proliferation[49]. To count CFU-F colonies, the cultures were stained with 0.1% Toluidine blue in 4% formalin eight days after plating. Osteogenic, adipogenic and chondrogenic differentiation were assessed using StemPro Differentiation kits (Gibco).

Quantitative reverse transcription PCR

For quantitative PCR (qPCR), cells were flow cytometrically sorted from enzymatically dissociated bone marrow into Trizol (Invitrogen). RNA was extracted and reverse transcribed into cDNA using SuperScript III

(Invitrogen) and random primers. qPCR was performed using a Roche LightCycler 480. The primers used for qPCR analysis included mouse *Oln*: 5′-AGG TCC TGG GAG GGA GTG-3′ and 5′-GGG CCT CCT GGA GAT TCT T-3′; *Actb*: 5′-GCT CTT TTC CAG CCT TCC TT-3′ and 5′-CTT CTG CAT CCT GTC AGC AA-3′.

Long-term competitive reconstitution assays

Recipient mice were irradiated using an XRAD 320 X-ray irradiator (Precision X-Ray) with two doses of 540 rad at least 4 h apart. C57BL/Ka (CD45.1/CD45.2 heterozygous) mice were used as recipients. Five-hundred-thousand unfractionated bone marrow cells from donor (CD45.2) and competitor (CD45.1) mice were mixed and injected intravenously through the retro-orbital venous sinus. Recipient mice were bled from 4 to 16 weeks after transplantation to examine the levels of donor-derived myeloid, B and T cells in their blood. Red blood cells were then lysed with ammonium chloride potassium buffer before antibody staining. The antibodies used to analyse donor chimerism in the blood were anti-CD45.1 (A20), anti-CD45.2 (104), anti-Gr1 (8C5), anti-Mac1 (M1/70), anti-B220 (6B2) and anti-CD3 (KT31.1).

Bone fracture and ossicle formation

As previously described[13], a stainless steel wire was inserted into the intramedullary canal of the femur through the knee after anaesthesia, and the femur was fractured mid-diaphysis by three-point bending. Buprenorphine was injected every 12 h up to 72 h after the surgery. Mice were analysed 2 weeks after the surgery, using the contralateral femur as an internal control.

As previously described[13,29], 2×10^6 cultured mouse primary CFU-F cells were seeded into collagen sponges (Gelfoam), incubated at 37 °C for 90 min, and then transplanted subcutaneously into NOD–SCID *Il2rg*$^{-/-}$ (NSG) mice. The ossicles formed by these cells were analysed eight weeks after transplantation by cryosectioning, Haematoxylin and eosin staining.

Micro-computed tomography analysis

Femurs from sex-matched littermates were fixed in 4% PFA overnight at 4 °C, then the bones were washed 4 times with 70% ethanol and stored in 70% ethanol until scanned using a Scanco Medical μCT 35. Femurs were scanned at an isotropic voxel size of 3.5 μm, with peak tube voltage of 55 kV and current of 0.145 mA (μCT 35; Scanco). A three-dimensional Gaussian filter ($s = 0.8$) with a limited, finite filter support of one was used to suppress noise. A threshold of 263–1,000 was used to segment mineralized bone from air and soft tissues. Cortical bone parameters were measured by analysing 100 slices in mid-diaphysis femurs.

RNA-seq analysis

Cells were sorted into RLT buffer (Qiagen RNAeasy Plus Micro kit) and RNA was purified according to the manufacturer's instructions. RNA quality was validated using a Pico Bioanalyzer. Libraries were generated using SMARTer Stranded Total RNA-Seq kit–Pico Input Mammalian (Clonetech). Library fragment size was measured using D1000 Screen Tape (Agilent) and RNA was quantified using the Qubit RNA assay kit (Life Technologies). Libraries were sequenced using an Illumina Next-Seq 500. The quality of RNA-seq raw reads was checked using FastQC 0.11.5. Raw reads were trimmed using Cutadapt 2.3 and mapped to the Ensembl GRCm38 mouse genome using TopHat 2.1.1 with Bowtie2 2.2.3. Mapped reads were quality-filtered using SAMtools 1.9.0 and quantified using HTSeq 0.9.1. Differential expression was assessed using DESeq2 1.24.0 with R 3.6.1. Gene set enrichment analysis of the filtered, DESeq2-normalized counts was performed using GSEA 4.0.3 with the osteogenesis gene list PAMM-026Z and the adipogenesis gene list PAMM-049Z from Qiagen's RT^2 Profiler PCR Array.

Voluntary running and hindlimb unloading

Mice were individually housed in standard polycarbonate mouse cages (Fisher Scientific) containing a 4.75-inch diameter stainless steel running wheel for 4 weeks. To mechanically unload mouse hindlimbs, 8-week-old mice were outfitted with tail harnesses and suspended from an overhead pulley system in customized cages, as previously described[33] (schematic in Extended Data Fig. 8c). The mice ambulated within the cage using their forelimbs, which remained in contact with the cage floor, but their hindlimbs were suspended in the air and consequently could not generate ground reaction forces. Control mice were housed individually with tail harnesses attached to the overhead pulley system as well, but with both forelimbs and hindlimbs in contact with the cage floor. Food and water were provided on the cage floor. Mice were suspended continuously for two weeks, then analysed.

Listeria infection

Listeria monocytogenes strain 10403S was freshly inoculated onto a brain-heart infusion (BHI) agar plate. A single colony was chosen and expanded in BHI broth at 37 °C with shaking at 200 rpm. For infection, bacteria were sub-cultured and grown to log phase (optical density at 600 nm of 0.6–1) on the day of infection, washed, and resuspended in PBS. Mice were administered 2×10^9 colony-forming units (CFU) of *Listeria* by oral gavage, or 2×10^6 CFU of *Listeria* intraperitoneally. To quantify bacteria, spleens were collected from infected mice and homogenized using FastPrep-24 5G (MP Biomedicals) in PBS containing 0.1% Triton X-100, followed by serial dilutions using PBS and plating onto BHI agar plates. Colonies were counted after 24 h of growth at 37 °C. The intracellular IFN-γ level in T cells was measured as previously described[50]. Splenocytes were stimulated with 50 ng ml^{-1} phorbol 12-myristate 13-acetate and 1 μM ionomycin in the presence of 1 μg ml^{-1} brefeldin A for 4.5 h, followed by staining with antibody against CD3. The cells were fixed with 2% paraformaldehyde, permeabilized with 0.1% saponin, and stained for IFNγ, then IFNγ levels were analysed by flow cytometry in CD3$^+$ cells. The mice were processed and data were collected in a manner blinded to sample identity.

Electrophysiology

Oln-mTomato$^+$ cells were isolated by flow cytometry and cultured for 2 days in 6-well plates pre-coated with 100 ng ml^{-1} of fibronectin (Sigma), with DMEM-low glucose (Gibco) plus 20% fetal bovine serum (Sigma F2442), 10 mM ROCK inhibitor (Y-27632, Selleck), and 1% penicillin/streptomycin (Invitrogen) at 37 °C in a low oxygen environment (to promote cell survival) within gas-tight chambers (Billups–Rothenberg) flushed with 1% O_2 and 6% CO_2 (balance Nitrogen). After that, the cells were transferred to a regular 37-°C incubator with 5% CO_2, cultured for 3 additional days, detached with TrypLE Express (Thermo Scientific) and replated on glass coverslides (Carolina Biological Supply) at 50–70% confluency for 16 h before electrophysiological recordings. Single channel current recordings of endogenous PIEZO1 were performed using an Axopatch 200B amplifier and Digidata 1550B digitizer (Molecular Devices). Currents were acquired with pClamp 10.7 software at a sampling frequency of 10 kHz. Recording patch pipettes of borosilicate glass were pulled and fire-polished to a tip resistance of 4–6 MΩ. The external bath solution contained 140 mM KCl, 10 mM HEPES, 1 mM MgCl2, 10 mM glucose, pH 7.3 (pH adjusted with KOH). The pipette solution contained: 130 mM NaCl, 5 mM KCl, 10 mM HEPES, 10mM tetraethylammonium chloride (TEA-Cl), 1 mM $CaCl_2$, 1 mM $MgCl_2$, pH 7.3 (pH adjusted with NaOH). The bath electrode was grounded, while the pipette electrode was active, such that at positive applied potential, cations moved from pipette to bath, and vice versa. Mechanical stimulation was applied via recording pipette using a high-speed pressure clamp system (ALA Scientific Instruments). Single channel events are shown as upward deflections at +60 mV representing inward currents. The single channel data were analysed using Clampfit 10.7. All point current histograms (ranging from 5 to 10 s recorded stretch) were constructed in Clampfit. The single channel current values were extracted after fitting the Gaussian function to the data. Data are presented as mean ± s.d. Each data point is at least an average of 5 to

10 individual recordings. Open probability was calculated exclusively from the records, where at least 10 s of data were recorded both before and after pressure application.

Statistical methods

In each type of experiment, multiple independent experiments were performed using different mice on different days. Mice were allocated to experiments randomly and samples were processed in an arbitrary order, but formal randomization techniques were not used. Before analysing the statistical significance of differences among treatments, we tested whether the data were normally distributed and whether variance was similar among treatments. To test for normal distribution, we performed the Shapiro–Wilk test when $3 \leq n < 20$ or the D'Agostino Omnibus test when $n \geq 20$. To test whether variability significantly differed among treatments, we performed *F*-tests (for experiments with two treatments) or Levene's median tests (for more than two treatments). When the data significantly deviated from normality or variability significantly differed among treatments, we $\log_2$-transformed the data and tested again for normality and variability. If the transformed data no longer significantly deviated from normality and equal variability, we performed parametric tests on the transformed data. If transformed data still significantly deviated from normality or equal variability, we performed non-parametric tests on the non-transformed data.

All the statistical tests we used were two-sided, where applicable. To assess the statistical significance of a difference between two treatments, we used paired *t*-tests (when mice were littermates and a parametric test was appropriate), Wilcoxon signed rank tests (when mice were littermates and a non-parametric test was appropriate), *t*-tests (when mice were not littermates and a parametric test was appropriate), or Mann–Whitney tests (when mice were not littermates and a non-parametric test was appropriate). Multiple *t*-tests (parametric or non-parametric) were followed by Holm–Sidak's multiple-comparisons adjustment. To assess the statistical significance of differences between more than two treatments, we used repeated measures one-way or two-way ANOVA (when mice were littermates and/or cells were from same mice, and a parametric test was appropriate) followed by Tukey's, Dunnet's, or Sidak's multiple-comparisons adjustment. To assess the significance of frequency differences within contingency tables that involved multiple experiments we used Cochran–Mantel–Haenszel tests. To assess the significance of survival differences we used the Mantel–Cox log-rank test.

All statistical analyses were performed with Graphpad Prism 8.3 or R 3.5.1 with the fBasics package. All data represent mean ± s.d. Samples sizes were not pre-determined on the basis of statistical power calculations but were based on our experience with these assays.

Reporting summary

Further information on research design is available in the Nature Research Reporting Summary linked to this paper.

Data availability

Source data files are provided with this paper. RNA sequencing data have been submitted to the NCBI Sequence Read Archive (SRA), accession number BioProject PRJNA626582. Source data are provided with this paper.

44. DeFalco, J. et al. Virus-assisted mapping of neural inputs to a feeding center in the hypothalamus. *Science* **291**, 2608–2613 (2001).
45. Madisen, L. et al. A robust and high-throughput Cre reporting and characterization system for the whole mouse brain. *Nat. Neurosci.* **13**, 133–140 (2010).
46. Daigle, T. L. et al. A suite of transgenic driver and reporter mouse lines with enhanced brain-cell-type targeting and functionality. *Cell*. **174**, 465–480 (2018).
47. Cahalan, S. M. et al. Piezo1 links mechanical forces to red blood cell volume. *eLife* **4**, e07370 (2015).
48. Muzumdar, M. D., Tasic, B., Miyamichi, K., Li, L. & Luo, L. A global double-fluorescent Cre reporter mouse. *Genesis* **45**, 593–605 (2007).
49. Morrison, S. J. et al. Culture in reduced levels of oxygen promotes clonogenic sympathoadrenal differentiation by isolated neural crest stem cells. *J. Neurosci.* **20**, 7370–7376 (2000).
50. Gao, D. et al. Activation of cyclic GMP–AMP synthase by self-DNA causes autoimmune diseases. *Proc. Natl Acad. Sci. USA* **112**, E5699–E5705 (2015).

Acknowledgements S.J.M. is a Howard Hughes Medical Institute (HHMI) Investigator, the Mary McDermott Cook Chair in Pediatric Genetics, the Kathryn and Gene Bishop Distinguished Chair in Pediatric Research, the director of the Hamon Laboratory for Stem Cells and Cancer, and a Cancer Prevention and Research Institute of Texas Scholar. This work was supported partly by the National Institutes of Health (DK118745 to S.J.M.). B.S. was supported by a Ruth L. Kirschstein National Research Service Award Postdoctoral Fellowship from the National Heart, Lung, and Blood Institute (F32 HL139016-01). A.T. was supported by the Leopoldina Fellowship Program (LPDS 2016-16) of the German National Academy of Sciences and the Fritz Thyssen Foundation. L.A.J. was supported by ARC Discovery grants (DP200101970, DE190100609). R.S. was supported by the UT Southwestern Medical Center Endowed Scholar Program, Welch Foundation Award (I-1965-20180324) and an American Heart Association scientist development grant (17SDG33410184). We thank H. Zeng and H. Taniguchi for providing the *Ai47* mice; N. Loof, T. Shih and the Moody Foundation Flow Cytometry Facility; and the BioHPC high-performance computing cloud at University of Texas Southwestern Medical Center for providing computational resources.

Author contributions B.S. and S.J.M. conceived the project, designed and interpreted experiments. B.S. performed most of the experiments, with technical assistance and discussions with A.T., J.M.U. and G.M.C. J.Z. and M.M.M. developed immunofluorescence staining protocols. E.D.N and R.S. performed the electrophysiological recordings measuring PIEZO1 channel activity. S.H. assisted in *Listeria* infection experiments. L.D. and N.K. helped to perform flow cytometry. Y.Y. and Z.H. assisted in establishing the hindlimb unloading model and helped with image acquisition. S.G., Y.J. and X.L. assisted B.S. to perform RNA sequencing and analysis. V.R. assisted in ossicle transplantation in NSG mice. E.C.M. and C.E. performed genotyping on mice. L.A.J. and Y.C.Z. provided advice on the mechanical properties of arterioles. Z.Z. performed bioinformatic and statistical analyses. B.S. and S.J.M. wrote the manuscript.

Competing interests The authors declare no competing interests.

Additional information

Supplementary information The online version contains supplementary material available at https://doi.org/10.1038/s41586-021-03298-5.

Correspondence and requests for materials should be addressed to S.J.M.

Peer review information *Nature* thanks Iannis Aifantis, Sara Wickstrom and the other, anonymous, reviewer(s) for their contribution to the peer review of this work. Peer reviewer reports are available.

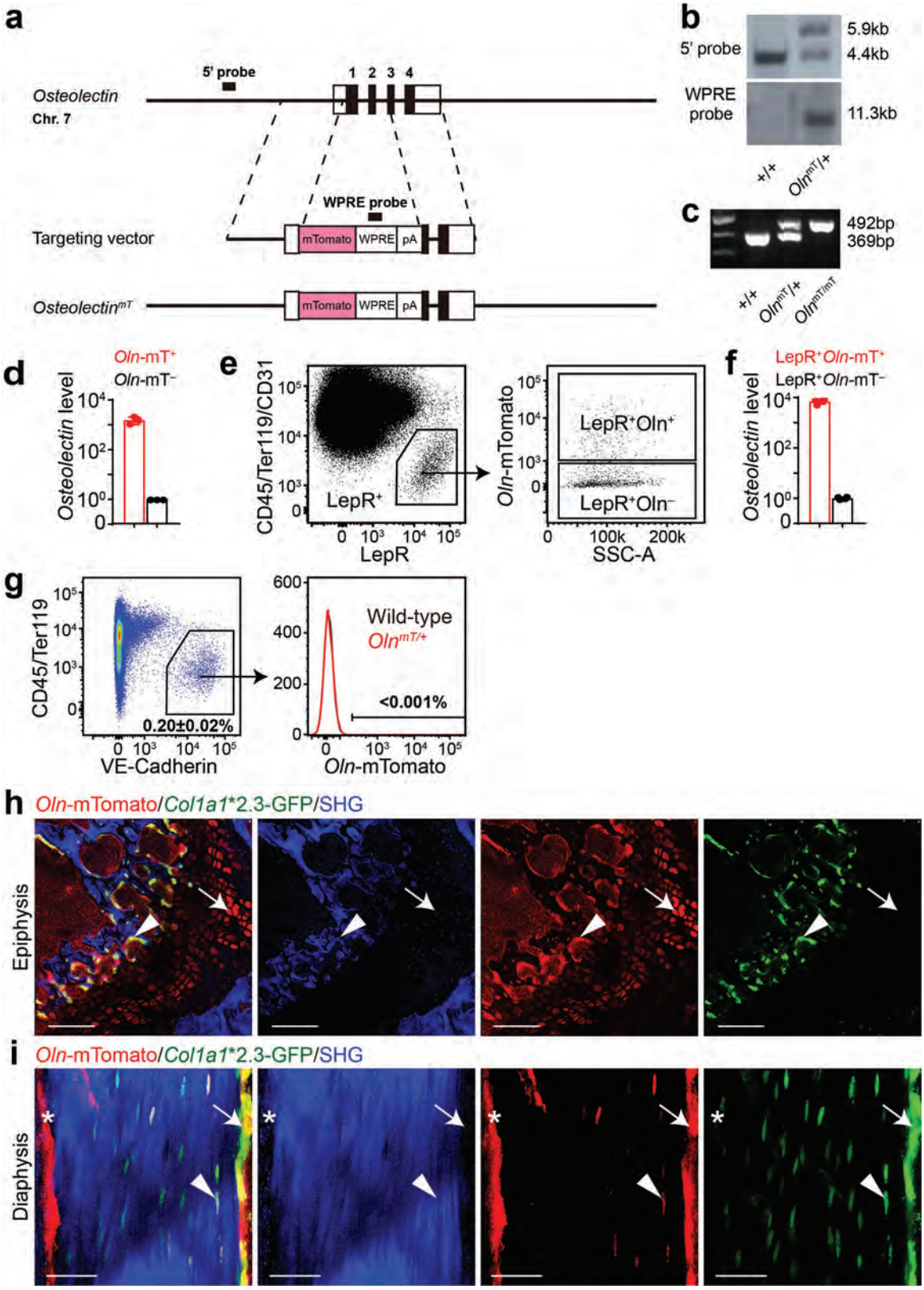

Extended Data Fig. 1 | See next page for caption.

Extended Data Fig. 1 | *Oln*^{mT} reporter mice showed that osteolectin is expressed by osteoblasts, osteocytes, and chondrocytes in addition to peri-arteriolar LEPR$^+$ stromal cells. a, The mouse *Oln* gene was modified to insert an mTomato-WPRE-pA cassette between the 5′ untranslated region and exon 3 to generate the targeting vector. These sites were selected to avoid disrupting conserved intronic sequences. Open boxes indicate untranslated regions and black boxes indicate translated regions of *Oln*. **b**, The targeted founder mouse (F_0) was identified by Southern blotting using 5′ and WPRE probes (black bars). **c**, PCR genotyping of genomic DNA confirmed germline transmission of the *Oln*^{mT} allele. Mice were backcrossed at least three times onto a C57BL/Ka background before analysis. **d**, *Oln* transcript levels by qPCR with reverse transcription (RT–qPCR) in *Oln*-mTomato$^+$ and *Oln*-mTomato$^-$ bone marrow cells (3 mice analysed in 3 independent experiments). **e**, Flow cytometry gates to distinguish *Oln*-mTomato$^+$LEPR$^+$ from *Oln*-mTomato$^-$LEPR$^+$ stromal cells in enzymatically dissociated bone marrow. **f**, *Oln* transcript levels by RT–qPCR in *Oln*-mTomato$^+$LEPR$^+$ and *Oln*-mTomato$^-$LEPR$^+$ bone marrow cells (4 mice analysed in 4 independent experiments). **g**, We did not detect *Oln*-Tomato in VE-cadherin-expressing bone marrow endothelial cells (4 mice per genotype analysed in 4 independent experiments). **h**, **i**, Femur epiphysis (**h**) and diaphysis (**i**) from *Oln*$^{mT/+}$;*Col1a1*2.3*-eGFP mice (images are representative of 3 independent experiments from 8- to 10-week-old mice). In **h**, the arrowhead points to *Oln*-tdTomato$^+$*Col1a1*2.3*-eGFP$^+$ osteoblasts in trabecular bone and the arrow points to *Oln*-tdTomato$^+$*Col1a1*2.3*-eGFP$^-$ hypertrophic chondrocytes in the growth plate (scale bar, 100 μm). **i**, *Oln*-tdTomato$^+$*Col1a1*2.3*-eGFP$^+$ osteoblasts at the endosteum (arrow), *Oln*-tdTomato$^+$ osteocytes (arrowhead), and *Oln*-tdTomato$^+$ periosteal cells (asterisk) (scale bars, 40 μm). All data represent mean ± s.d.

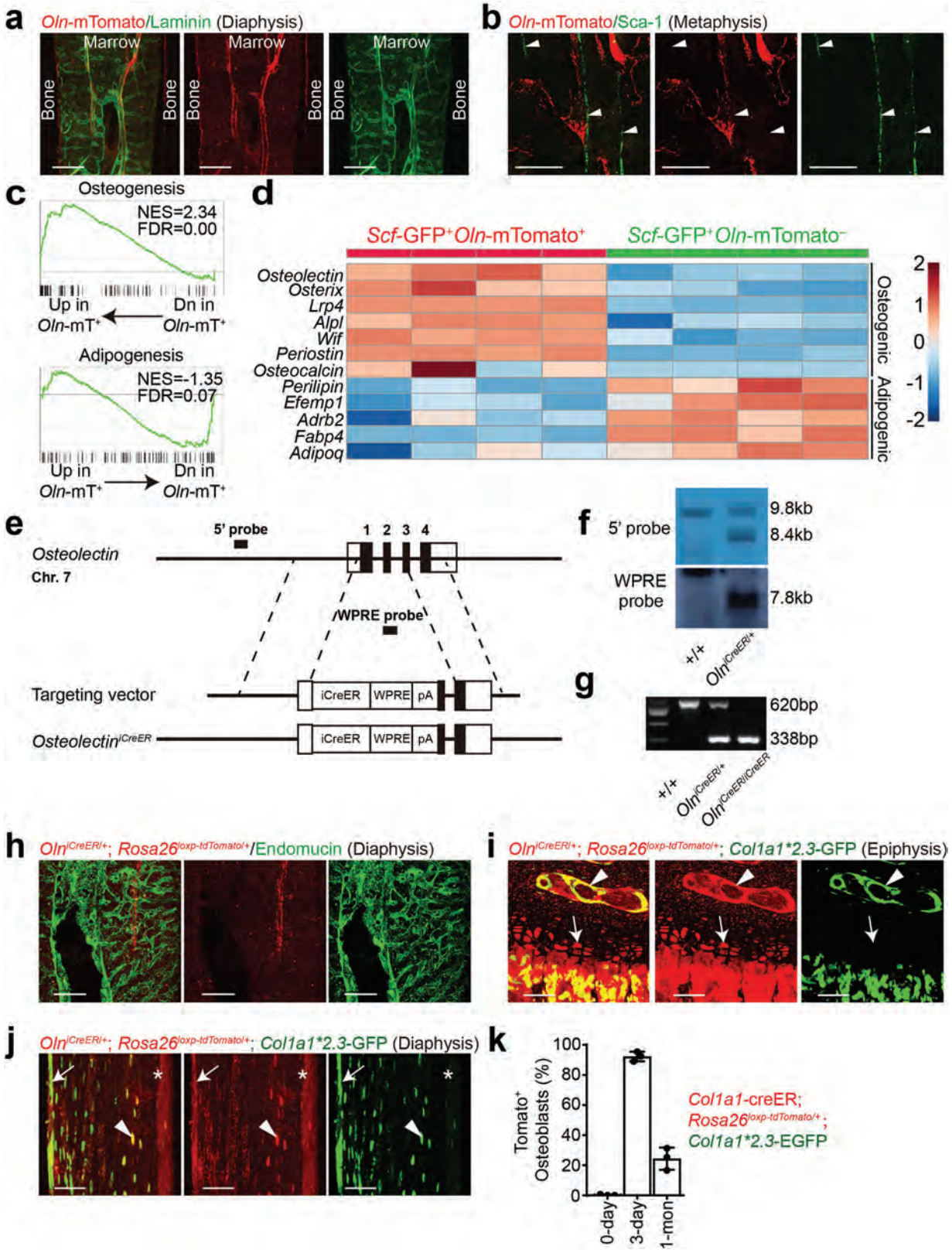

Extended Data Fig. 2 | See next page for caption.

Extended Data Fig. 2 | Bone marrow *Oln*-mTomato$^+$ cells localized mainly around arterioles in the diaphysis. a, A low-magnification view of the femur diaphysis showed *Oln*-mTomato$^+$ stromal cells associated with arterioles enriched in the centre of the marrow. In this image, arteriolar and sinusoidal blood vessels were distinguished based on size, morphology and continuity of the basal lamina, visualized using anti-laminin antibody staining as previously described[21] (images are representative of 3 independent experiments; scale bar, 200 μm). **b**, *Oln*$^{mT/+}$ femur bone marrow showing that, in contrast to the diaphysis (Fig. 1h), most SCA-1$^+$ arterioles were not surrounded by *Oln*-mTomato$^+$ stromal cells in the metaphysis. The *Oln*-mTomato$^+$ cells in this panel were osteoblasts and osteocytes associated with trabecular bone (scale bar, 500 μm). **c**, **d**, Gene set enrichment analysis showing significant enrichment of genes associated with osteogenesis in CD45$^-$Ter119$^-$CD31$^-$*Scf*-GFP$^+$*Oln*-mTomato$^+$ stromal cells and adipogenesis in CD45$^-$Ter119$^-$CD31$^-$*Scf*-GFP$^+$*Oln*-mTomato$^-$ stromal cells (FDR, false discovery rate; NES, normalized enrichment score; 4 mice analysed in 4 independent experiments). **e**, **f**, The mouse *Oln* gene was modified by inserting an iCreER-WPRE-pA cassette between the 5′ untranslated region and exon 3 to generate the targeting vector (**e**). These sites were selected to avoid disrupting conserved intronic sequences. Open boxes indicate untranslated regions and black boxes indicate translated regions of *Oln*. **f**, The targeted founder mouse (F_0) was identified by Southern blotting using 5′ and WPRE probes (black bars). **g**, PCR genotyping of genomic DNA confirmed germline transmission of the *Oln*^{iCreER} allele. Mice were backcrossed at least three times onto a C57BL/Ka background before analysis. **h**, Deep imaging of *Oln*$^{iCreER/+}$;*Rosa26*$^{loxp\text{-}tdTomato/+}$ femur bone marrow 3 days after tamoxifen administration at 2 months of age, showing that *Oln*-tdTomato$^+$ cells were exclusively peri-arteriolar in the diaphysis (images are representative of 3 independent experiments; scale bar, 200 μm). **i**, **j**, Deep imaging of the femur epiphysis (**i**) and diaphysis (**j**) one month after tamoxifen administration at 2 months of age (images are representative of 3 independent experiments). **i**, *Oln*-tdTomato$^+$ hypertrophic chondrocytes in the growth plate (arrow) and *Oln*-tdTomato$^+$*Col1a1*2.3*-eGFP$^+$ osteoblasts in trabecular bone (arrowhead; scale bar, 60 μm). **j**, *Oln*-tdTomato$^+$*Col1a1*2.3*-eGFP$^+$ osteoblasts at the endosteum (arrow), an *Oln*-tdTomato$^+$ osteocyte (arrowhead), and *Oln*-tdTomato$^+$ periosteal cells (asterisk; scale bars, 30 μm). **k**, *Col1a1*-CreER;*Rosa26*$^{loxp\text{-}tdTomato/+}$;*Col1a1*2.3*-eGFP mice were treated with tamoxifen at 2 months of age and the percentage of *Col1a1*2.3*-eGFP$^+$ osteoblasts that were tdTomato$^+$ was assessed 3 days to 1 month later (3 mice per time point analysed in 3 independent experiments). All data represent mean ± s.d.

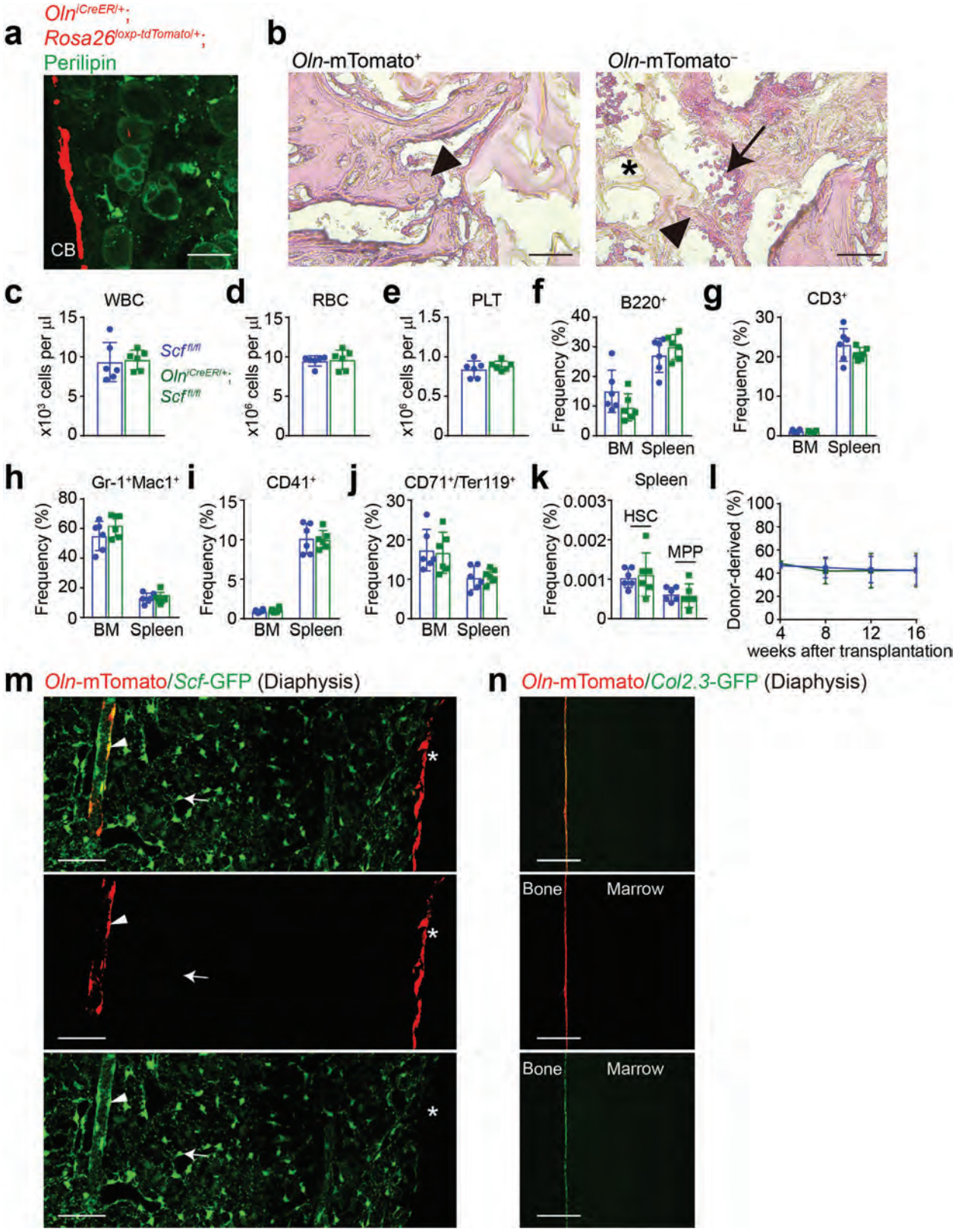

Extended Data Fig. 3 | See next page for caption.

Extended Data Fig. 3 | Osteolectin$^+$ cells create a niche for CLPs but not other haematopoietic stem or progenitor cells. a, Two-month-old *Oln$^{iCreER/+}$;Rosa26$^{loxp\text{-}tdTomato/+}$* mice were sublethally irradiated 3 days after tamoxifen administration. Two weeks later, none of the adipocytes in the bone marrow were tdTomato$^+$ (image representative of 3 independent experiments; scale bar, 60 μm). **b**, Representative H&E stained sections from ossicles formed by *Oln*-mTomato$^+$ (left) or *Oln*-mTomato$^-$ (right) stromal cells sorted from *Oln$^{mT/+}$* mice showing bone (arrowheads), haematopoietic cells (arrow), and adipocytes (asterisk; images are representative of 5 independent experiments; scale bar, 100 μm). **c**–**e**, *Oln$^{iCreER/+}$;Scf$^{fl/fl}$* and *Scf$^{fl/fl}$* littermate controls were treated with tamoxifen at two months of age. One month later, blood from *Oln$^{iCreER/+}$;Scf$^{fl/fl}$* mice showed normal white blood cell (**c**), red blood cell (**d**) and platelet (**e**) counts (6 mice per genotype analysed in three independent experiments). **f**–**k**, *Oln$^{iCreER/+}$;Scf$^{fl/fl}$* mice and littermate controls exhibited no significant differences in the frequencies of B220$^+$ B cells (**f**), CD3$^+$ T cells (**g**), Gr-1$^+$Mac-1$^+$ myeloid cells (**h**), CD41$^+$ megakaryocyte lineage cells (**i**), CD71$^+$/Ter119$^+$ erythroid lineage cells (**j**) and HSCs or MPPs in the spleen (**k**; 6 mice per genotype analysed in 3 independent experiments). **l**, Bone marrow cells from *Oln$^{iCreER/+}$;Scf$^{fl/fl}$* mice and littermate controls gave similar levels of donor cell reconstitution upon competitive transplantation into irradiated mice (5 donor mice per genotype analysed in 3 independent experiments). The differences between *Oln$^{iCreER/+}$;Scf$^{fl/fl}$* and *Scf$^{fl/fl}$* mice were not statistically significant in **c**–**l**. **m**, *Oln$^{mT/+}$;Scf$^{GFP/+}$* femur bone marrow showing *Oln*-mTomato$^+$ osteoblasts at the endosteum were negative for *Scf*-GFP, while peri-arteriolar *Oln*-mTomato$^+$ stromal cells were positive for *Scf*-GFP (representative of 3 independent experiments; scale bar, 80 μm). **n**, *Oln$^{mT/+}$;Col1a1*2.3*-eGFP femur bone marrow showing *Col1a1*2.3*-eGFP$^+$ osteoblasts at the endosteum were *Oln*-mTomato$^+$ (representative of 3 independent experiments; scale bar, 100 μm). All data represent mean ± s.d. Statistical significance was assessed using matched-samples two-way ANOVA followed by Sidak's (**c**–**e**, **k**, **l**) or Tukey's (**f**–**j**) multiple-comparisons tests.

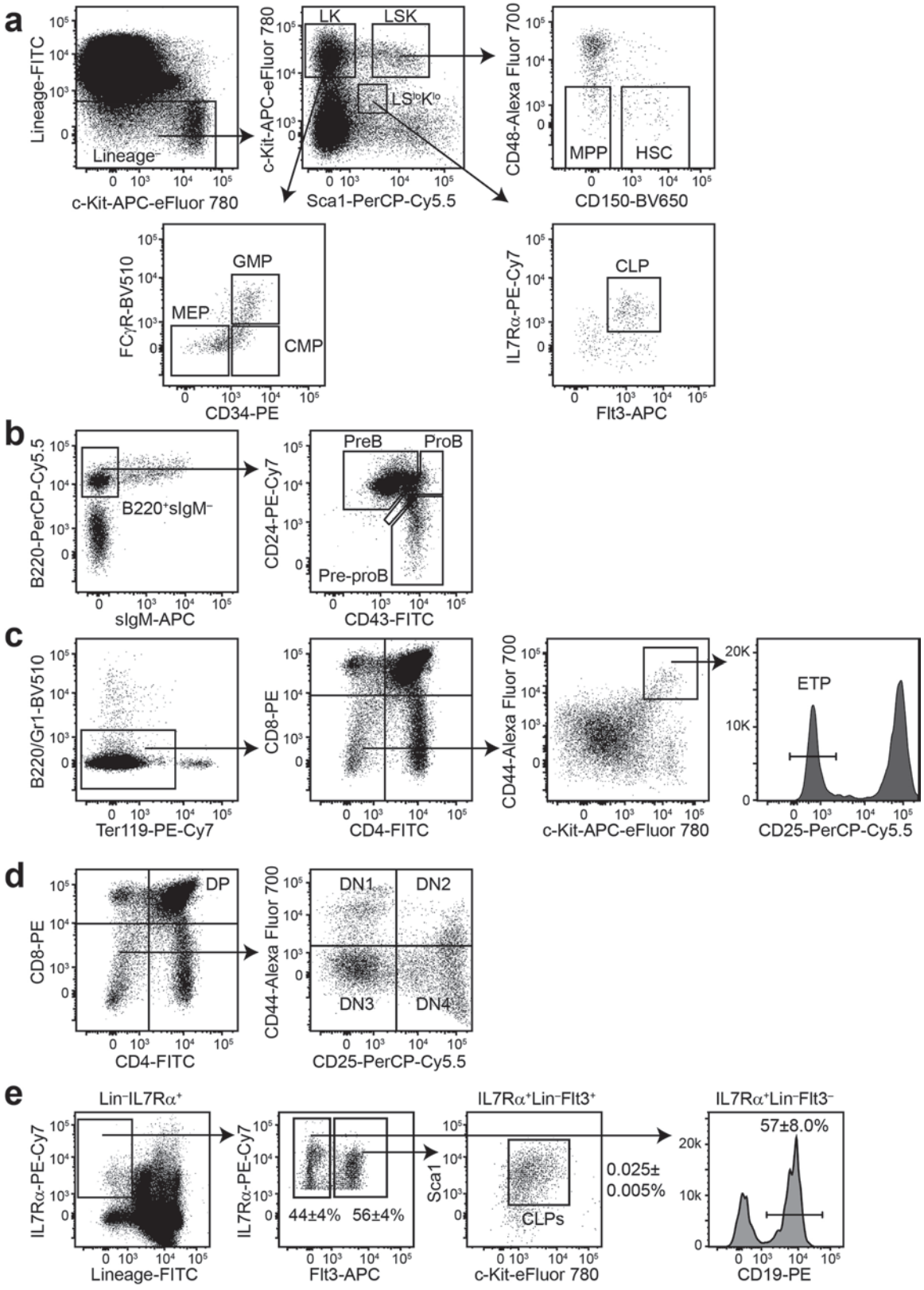

Extended Data Fig. 4 | Flow cytometry gating strategy for the isolation of haematopoietic stem and progenitor cell populations. a–**d**, Representative flow cytometry gates used to identify the haematopoietic stem and progenitor cell populations in the bone marrow (**a**, **b**), and T lineage progenitors in the thymus (**c**, **d**). The markers used to identify each of the cell populations characterized in this study are listed in Supplementary Table 1. **e**, Representative flow cytometry gates showing that more than 50% of IL7Rα$^+$lineage$^-$ cells were Lin$^-$SCA1^{low}KIT^{low}IL7Rα$^+$Flt3$^+$ CLPs and most of the non-CLP IL7Rα$^+$lineage$^-$ (Flt3$^-$) cells were CD19$^+$, probably other early B lineage progenitors (4 mice analysed in 3 independent experiments). All data represent mean ± s.d.

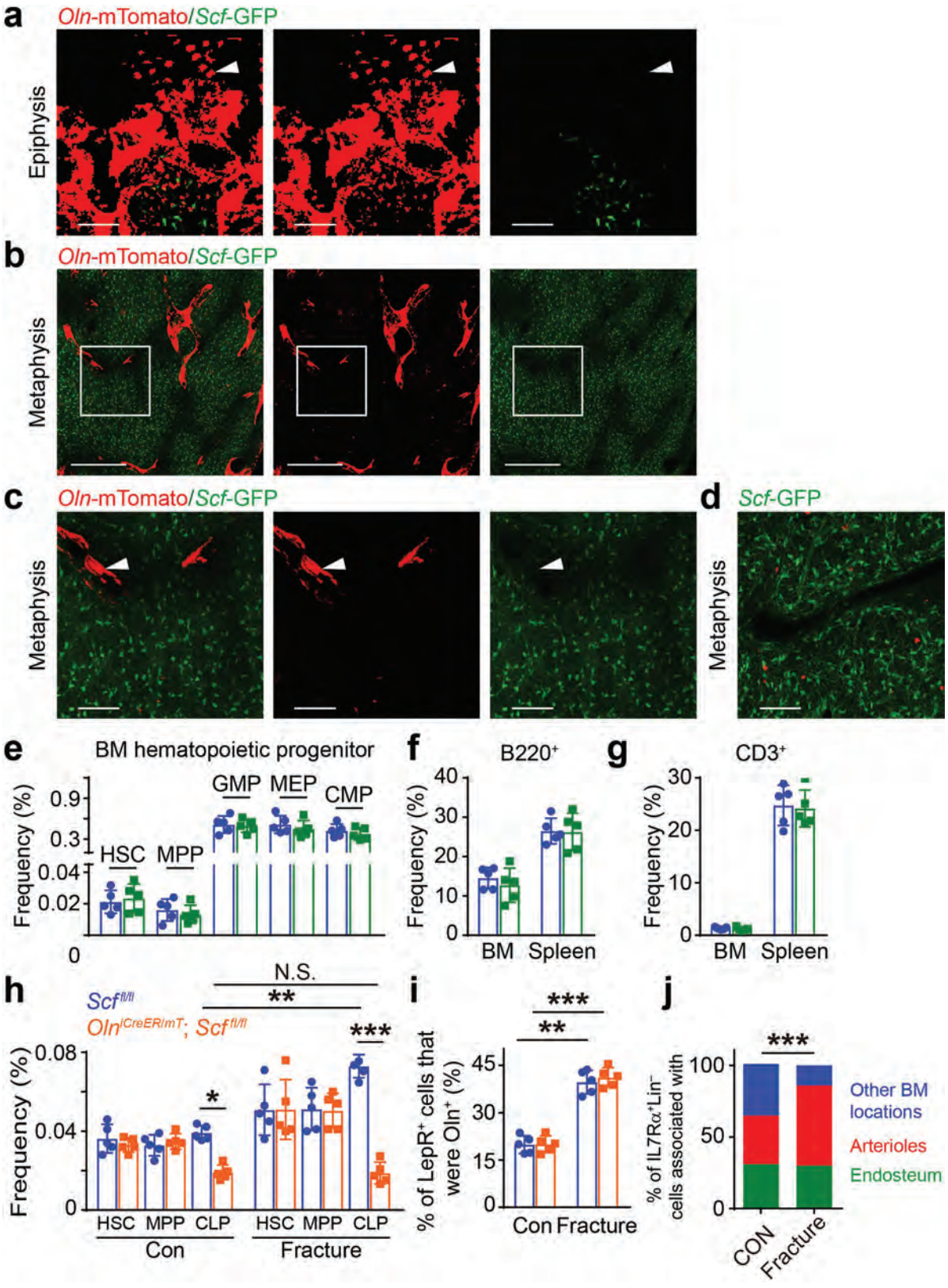

Extended Data Fig. 5 | See next page for caption.

Extended Data Fig. 5 | *Oln*-mTomato$^+$ osteoblasts and osteocytes in the metaphysis do not express *Scf*-GFP and *Oln*-mTomato$^+$ cells in the diaphysis expand during fracture healing. The differences among treatments in cell frequencies were also evident in absolute numbers. (**a**–**c**) Epiphysis (**a**) and metaphysis (**b**, **c**) of $Oln^{mT/+}$;$Scf^{GFP/+}$ femur bone marrow showing that hypertrophic chondrocytes (arrowhead in **a**; scale bars, 30μm) as well as osteoblasts and osteocytes associated with trabecular bone (arrowhead in **c**) were negative for *Scf*-GFP (images are representative of 3 independent experiments; scale bars, 400 μm (**b**) and 100 μm (**c**)). Most of the *Oln*-Tomato staining in the metaphysis reflects *Col1a1*2.3-GFP*$^+$ osteoblasts and osteocytes associated with trabecular bone, as shown in Fig. 1d and Extended Data Fig. 2b. The boxed area in **b** is magnified in **c**. **d**, Image of the metaphysis of $Scf^{GFP/+}$ femur bone marrow showing limited non-specific staining by anti-tdTomato antibody (scale bar, 100 μm). **e**–**g**, $Oln^{iCreER/+}$;$Scf^{fl/fl}$ and $Scf^{fl/fl}$ littermate control mice were fed tamoxifen chow from 2–4 months of age. They exhibited no significant differences in the frequencies of HSCs, MPPs, GMPs, MEPs, or CMPs in the bone marrow (**e**), B220$^+$ B cells (**f**), or CD3$^+$ T cells (**g**) in the bone marrow or spleen. The differences between $Oln^{iCreER/+}$; $Scf^{fl/fl}$ and $Scf^{fl/fl}$ mice were not statistically significant in **e**–**g** (5 mice per genotype analysed in 3 independent experiments). **h**, **i**, Three days after tamoxifen, femurs were fractured in two-month-old $Oln^{mT/iCreER}$;$Scf^{fl/fl}$ mice and $Oln^{mT/+}$;$Scf^{fl/fl}$ littermate controls then the bone marrow was analysed two weeks later. **i**, HSC and MPP frequencies did not significantly change during fracture healing. **h**, By contrast, CLP frequencies significantly increased in $Oln^{mT/+}$;$Scf^{fl/fl}$ control but not in $Oln^{mT/iCreER}$;$Scf^{fl/fl}$ mice. The frequency of osteolectin$^+$ cells significantly increased in both $Oln^{mT/iCreER}$;$Scf^{fl/fl}$ mice and $Oln^{mT/+}$;$Scf^{fl/fl}$ controls (**i**); 5 mice per genotype analysed in 3 independent experiments). **j**, Localization of IL7Rα$^+$Lineage$^-$ lymphoid progenitors in the marrow of the fractured as compared to control (CON) femur (4 mice per treatment analysed in 4 independent experiments). All data represent mean ± s.d. Statistical significance was assessed using matched-samples two-way ANOVAs followed by Sidak's (**e**–**i**) or Tukey's multiple-comparisons tests (**h**), or Cochran–Mantel–Haenszel test (**j**).

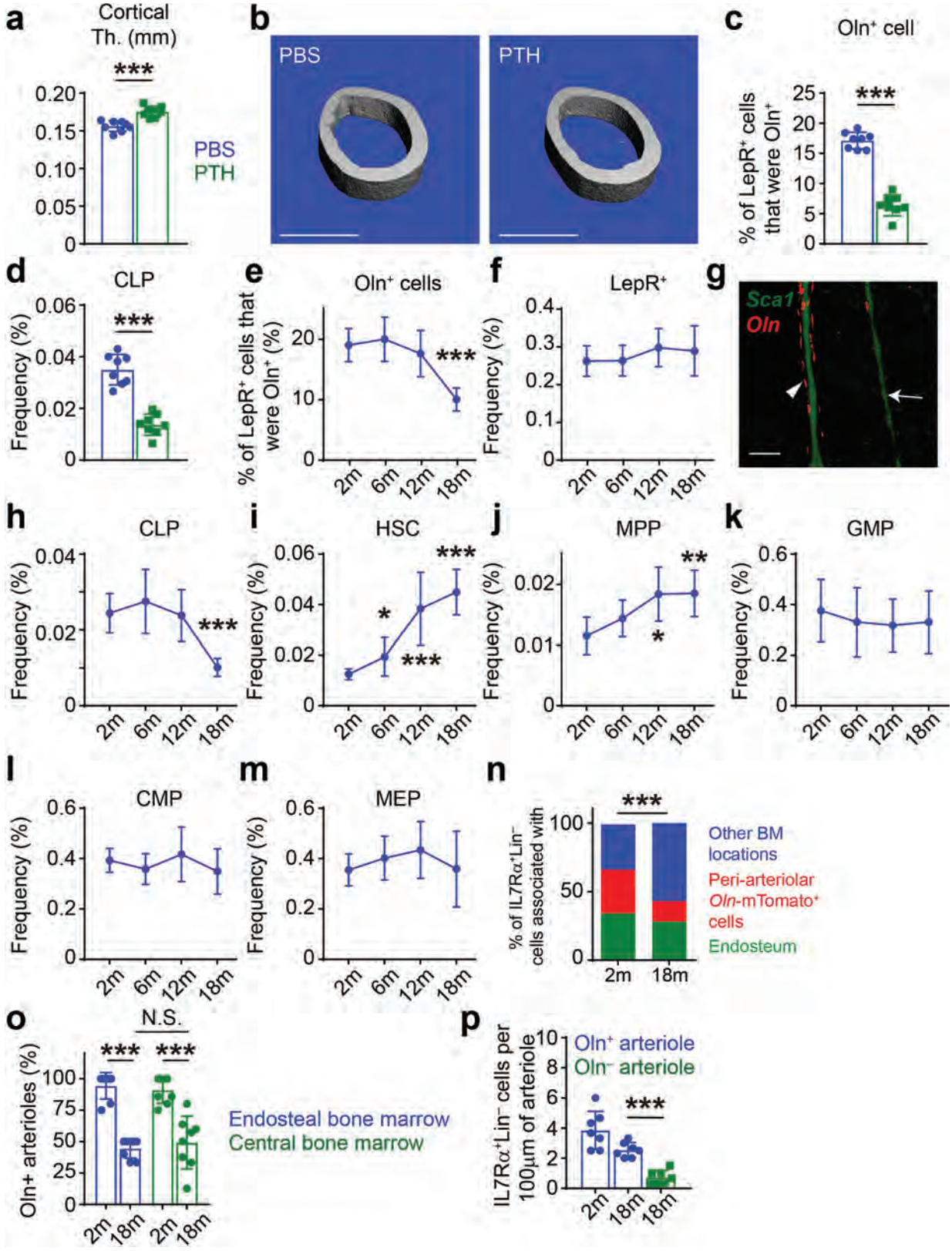

Extended Data Fig. 6 | See next page for caption.

Extended Data Fig. 6 | CLPs and peri-arteriolar osteolectin$^+$ cells are depleted during ageing but most other haematopoietic stem and progenitor cell populations are not. The differences among treatments in cell frequencies were also evident in absolute numbers. **a**–**d**, *Oln*$^{mT/+}$ mice received daily subcutaneous injections with PBS or 40 μg/kg human PTH for 28 days. PTH treated mice exhibited significantly thicker cortical bone (**a**, **b**) and significant reductions in the frequencies of osteolectin$^+$ cells (**c**) and CLPs (**d**) (8 mice per treatment analysed in 4 independent experiments). Micro CT images (**b**; scale bar, 800 μm) of cortical bone are representative of 8 independent experiments. **e**, **f**, The frequency of LEPR$^+$ cells (**e**) and the percentage of LEPR$^+$ cells that were *Oln*-mTomato$^+$ (**f**) in *Oln*$^{mT/+}$ bone marrow at 2 to 18 months of age (8 mice per time point analysed in 4 independent experiments). **g**, Femur bone marrow from an 18-month-old *Oln*$^{mT/+}$ mouse showing an arteriole surrounded by *Oln*-mTomato$^+$ cells (arrowhead) and an arteriole lacking *Oln*-mTomato$^+$ cells (arrow) in the diaphysis (image is representative of 4 independent experiments; scale bar, 100 μm). **h**, The frequency of CLPs in *Oln*$^{mT/+}$ mice at 2 to 18 months of age. **i**–**m**, During ageing, the frequencies of HSCs (**i**) and MPPs (**j**) in the bone marrow increased while the frequencies of GMPs (**k**), CMPs (**l**), and MEPs (**m**) did not significantly change (8 mice per time point analysed in 4 independent experiments). **n**, Localization of IL7Rα$^+$Lineage$^-$ cells in the bone marrow of 2- and 18-month-old mice (7 mice per time point analysed in 3 independent experiments). **o**, Ageing significantly depleted osteolectin$^+$ cells associated with arterioles in both endosteal and non-endosteal regions of diaphysis bone marrow (8 mice per time point analysed in 4 independent experiments). **p**, Number of IL7Rα$^+$Lineage$^-$ cells per 100 μm of osteolectin$^+$ or osteolectin$^-$ arteriole at 2 and 18 months of age (7 mice per time point analysed in 3 independent experiments). All data represent mean ± s.d. Statistical significance was assessed using paired *t*-tests (**a**, **c**, **d**, **o**, **p**), one-way ANOVA followed by Dunnett's multiple-comparisons test (**e**), matched-samples two-way ANOVAs followed by Dunnett's multiple-comparisons tests (**f**, **h**–**m**), Cochran–Mantel–Haenszel test (**n**) or Mann–Whitney tests followed by Holm–Sidak's multiple-comparisons adjustments (**o**).

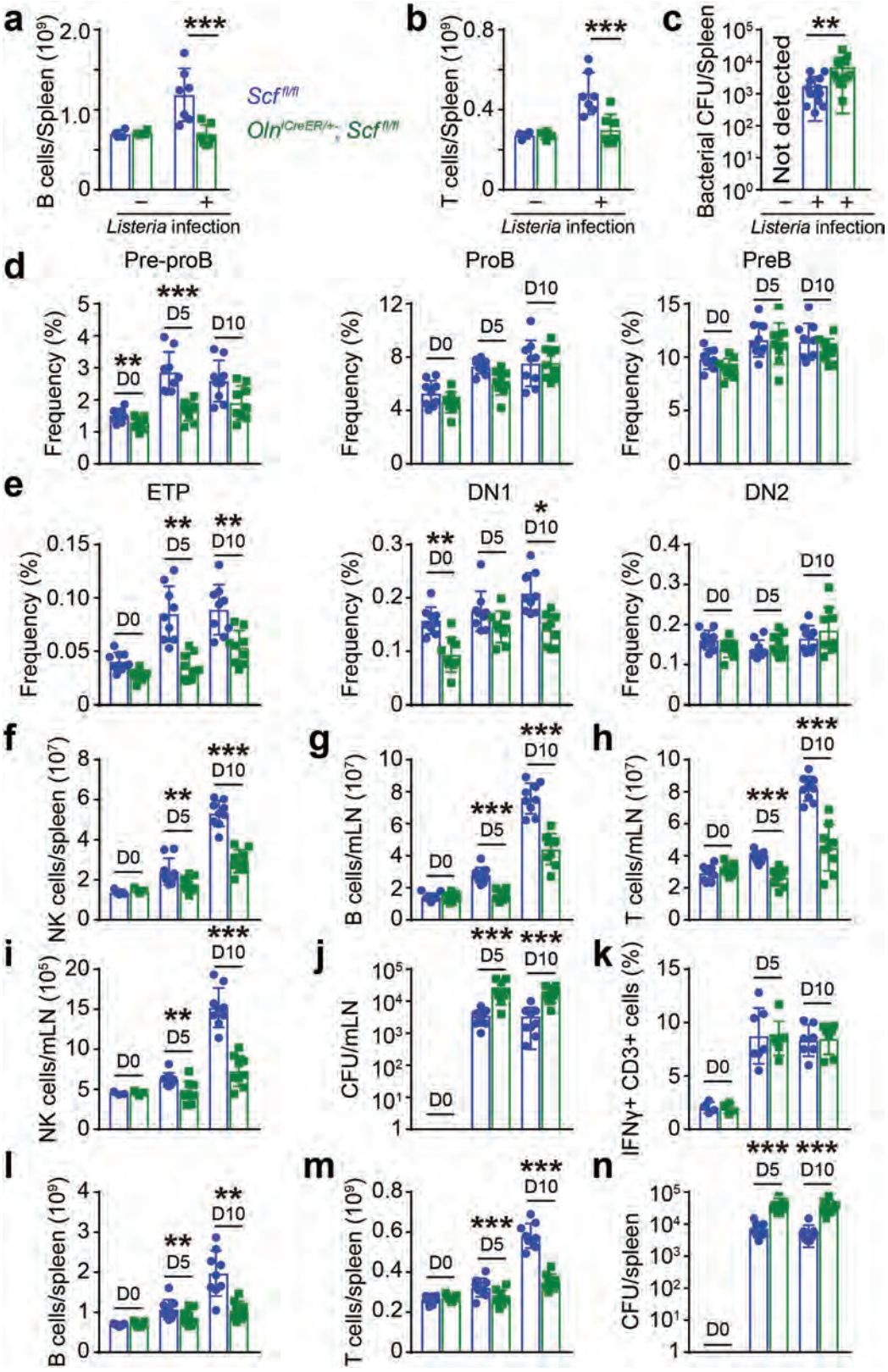

Extended Data Fig. 7 | See next page for caption.

Extended Data Fig. 7 | *Oln*$^{iCreER/+}$;*Scf*$^{fl/fl}$ mice exhibited reduced lymphopoiesis and impaired bacterial clearance after *Listeria* infection. The same differences that were evident among treatments in the frequencies of cell populations were also evident in absolute numbers. **a**–**c**, *Oln*$^{iCreER/+}$;*Scf*$^{fl/fl}$ mice and littermate controls were treated with tamoxifen at 2 months of age and then 3 days later were administered *Listeria* orally. Relative to *Scf*$^{fl/fl}$ littermate controls, *Oln*$^{iCreER/+}$;*Scf*$^{fl/fl}$ mice had decreased B (**a**) and T (**b**) cell counts in the spleen 5 days after *Listeria* infection and increased bacterial CFUs in the spleen 10 days after infection (**c**; 11-16 mice per genotype analysed in 3 independent experiments). **d**–**k**, *Oln*$^{iCreER/+}$;*Scf*$^{fl/fl}$ and *Scf*$^{fl/fl}$ littermate controls were fed tamoxifen from 2 to 4-months of age then 3 days later were administered *Listeria* intraperitoneally. Relative to *Scf*$^{fl/fl}$ littermate controls, *Oln*$^{iCreER/+}$;*Scf*$^{fl/fl}$ mice exhibited reduced frequencies of pre-proB cells, but not proB or preB cells, in the bone marrow (**d**) as well as ETPs and DN1 cells in the thymus (**e**) at 5 and/or 10 days after infection. *Oln*$^{iCreER/+}$;*Scf*$^{fl/fl}$ mice also exhibited reduced numbers of NK cells in the spleen (**f**) as well as B cells (**g**), T cells (**h**), and NK cells (**i**) in mesenteric lymph nodes (mLN) at 5 and 10 days after infection. **j**, *Oln*$^{iCreER/+}$;*Scf*$^{fl/fl}$ mice exhibited increased bacterial CFUs in mLN at 5 and 10 days after infection. **k**, The percentage of CD3$^+$ T cells that were IFNγ$^+$ did not significantly differ between the spleens of *Oln*$^{iCreER/+}$;*Scf*$^{fl/fl}$ mice and littermate controls (18–27 mice per genotype analysed in 3 independent experiments). **l**–**n**, Compared to *Scf*$^{fl/fl}$ controls, *Oln*$^{iCreER/+}$;*Scf*$^{fl/fl}$ mice had decreased spleen B (**l**) and T (**m**) cell counts, and increased spleen bacterial CFUs (**n**) at 5 and 10 days after infection with *Listeria* (21–27 mice per genotype analysed in 3 independent experiments). All data represent mean ± s.d. Statistical significance was assessed using matched-samples two-way ANOVA followed by Sidak's multiple-comparisons tests (**a**, **b**, **d**–**n**) or Wilcoxon matched-pairs test (**c**).

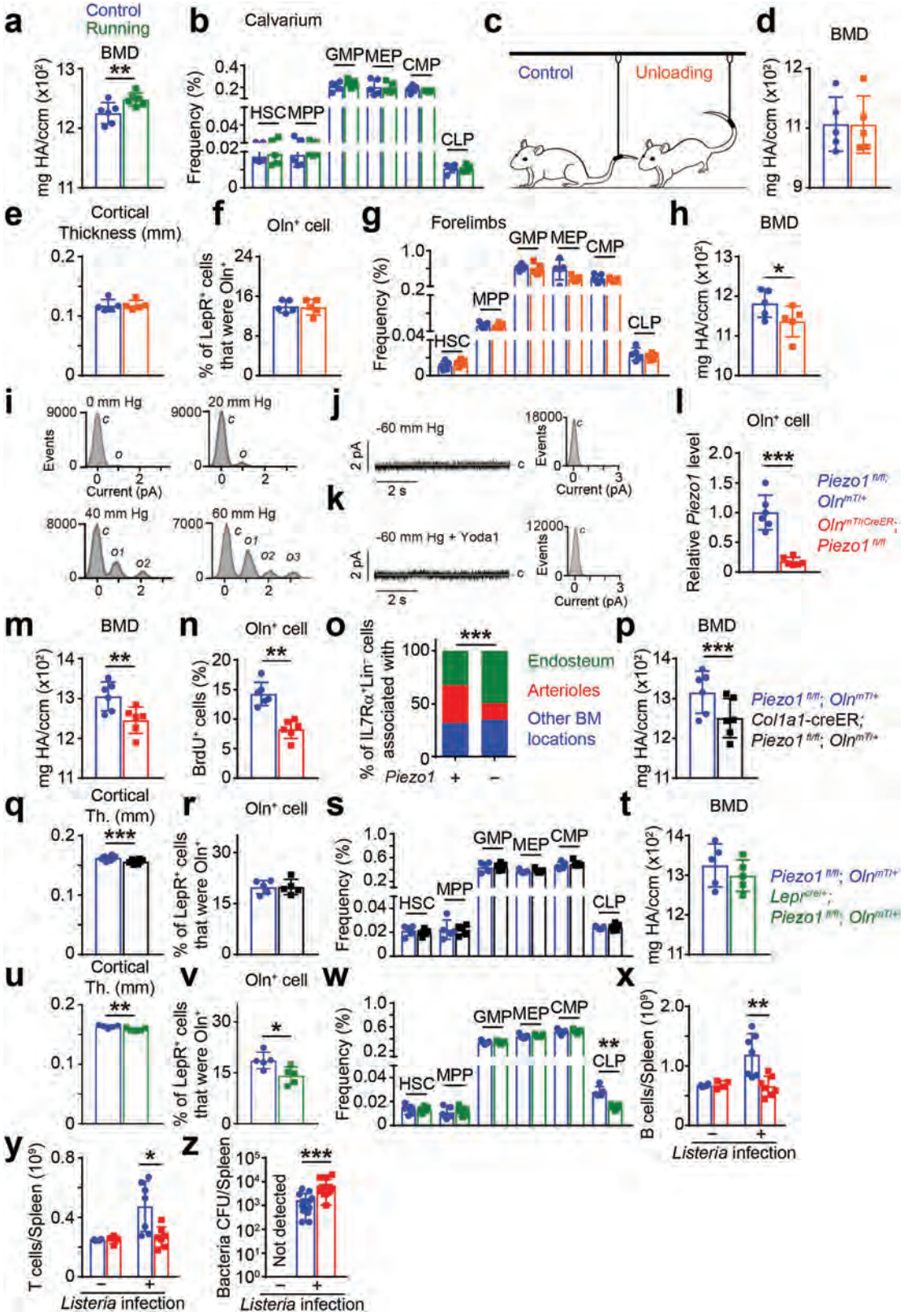

Extended Data Fig. 8 | See next page for caption.

Extended Data Fig. 8 | Mechanical stimulation is required for the maintenance of peri-arteriolar, but not peri-sinusoidal, niches for lymphoid progenitors in the bone marrow. a, The effect of voluntary running for 4 weeks on femoral cortical bone mineral density (6 mice per treatment analysed in 3 independent experiments). **b**, Voluntary running for 4 weeks did not significantly affect the frequencies of HSCs, MPPs, GMPs, MEPs, CMPs, or CLPs in calvarium bone marrow (5 mice per treatment analysed in 3 independent experiments). **c**–**h**, Hindlimb unloading (**c**) for 2 weeks did not significantly affect forelimb cortical bone mineral density (**d**), cortical thickness (**e**), the percentage of LEPR$^+$ cells that were *Oln*-mTomato$^+$ (**f**), or the frequencies of HSCs, MPPs, GMPs, MEPs, CMPs or CLPs in humerus bone marrow (**g**). **h**, Hindlimb unloading for 2 weeks significantly reduced hindlimb (femur) cortical bone mineral density (5 mice per treatment analysed in 3 independent experiments). **i**, All point current amplitude histograms of the electrical recordings in Fig. 4h. The single channel conductance was 15 ± 1 pS from the Gaussian fits to the amplitude histograms. The *y*-axis shows the number of events. **j**, **k**, Single channel current recordings and corresponding all point current histograms of *Piezo1* deficient *Oln*-mTomato$^+$ cells isolated from *Oln*$^{mT/iCreER}$*;Piezo1*$^{fl/fl}$ mice. The data were collected at -60 mm Hg applied pressure and at the holding potential of +60 mV, without (**j**) or with (**k**) 40 μM Yoda1 in the pipette. **l**, *Piezo1* transcript levels by RT–qPCR in *Oln*-mTomato$^+$ cells from *Oln*$^{mT/iCreER}$*;Piezo1*$^{fl/fl}$ and *Oln*$^{mT/+}$*;Piezo1*$^{fl/fl}$ control mice (6 mice per genotype analysed in 3 independent experiments). **m**, **n**, The effect of *Piezo1* deletion in osteolectin$^+$ cells on femoral cortical bone mineral density (**m**) and the percentage of osteolectin$^+$ cells that incorporated a 48-h pulse of BrdU (**n**; 6 mice per genotype analysed in 3 independent experiments). **o**, Location of IL7Rα$^+$Lineage$^-$ cells in the bone marrow of *Oln*$^{mT/iCreER}$*;Piezo1*$^{fl/fl}$ and *Oln*$^{mT/+}$*;Piezo1*$^{fl/fl}$ control mice (6 mice per genotype analysed in 3 independent experiments). **p**–**s**, We treated *Col1a1*-CreER*;Piezo1*$^{fl/fl}$*;Oln*$^{mT/+}$ mice and littermate controls with tamoxifen at 2 months of age and analysed them 1 month later. *Piezo1* deletion in osteoblasts significantly reduced femur bone mineral density (**p**) and cortical thickness (**q**) but not the frequencies of osteolectin$^+$ cells (**r**) or HSCs, MPPs, GMPs, MEPs or CLPs in the bone marrow (**s**; 5–6 mice per genotype analysed in 3 independent experiments). **t**–**w**, We analysed the femurs of *Lepr*$^{cre/+}$*;Piezo1*$^{fl/fl}$*;Oln*$^{mT/+}$ mice and littermate controls at 4 months of age and found that *Piezo1* deletion in LEPR$^+$ cells did not significantly reduce bone mineral density (**t**) but did reduce cortical thickness (**u**). *Piezo1* deletion in LEPR$^+$ cells also significantly reduced the frequencies of osteolectin$^+$ cells (**v**) and CLPs (**w**) without affecting the frequencies of HSCs, MPPs, GMPs, MEPs or CMPs (**w**) in the bone marrow (5 mice per genotype analysed in 3 independent experiments). **x**–**z**, Compared to *Scf*$^{fl/fl}$ littermate controls, *Oln*$^{iCreER/+}$*;Piezo1*$^{fl/fl}$ mice had decreased B (**x**) and T (**y**) cell counts in the spleen 5 days after oral *Listeria* infection and increased bacterial CFUs in the spleen 10 days after infection (**z**; 11-16 mice per genotype analysed in 3 independent experiments). All data represent mean ± s.d. Statistical significance was assessed using paired *t*-tests (**a**, **l**, **m**, **n**, **p**–**r**, **t**–**v**, **z**), matched-samples two-way ANOVAs followed by Sidak's (**b**, **d**–**f**, **h**, **s**, **w**–**y**) or Holm–Sidak's multiple-comparisons adjustment (**g**), or Cochran-Mantel–Haenszel test (**o**).

nature research

Corresponding author(s): Sean J. Morrison

Reporting Summary

Nature Research wishes to improve the reproducibility of the work that we publish. This form provides structure for consistency and transparency in reporting. For further information on Nature Research policies, see Authors & Referees and the Editorial Policy Checklist.

Statistical parameters

When statistical analyses are reported, confirm that the following items are present in the relevant location (e.g. figure legend, table legend, main text, or Methods section).

n/a	Confirmed	
☐	☒	The exact sample size (*n*) for each experimental group/condition, given as a discrete number and unit of measurement
☐	☒	An indication of whether measurements were taken from distinct samples or whether the same sample was measured repeatedly
☐	☒	The statistical test(s) used AND whether they are one- or two-sided *Only common tests should be described solely by name; describe more complex techniques in the Methods section.*
☒	☐	A description of all covariates tested
☐	☒	A description of any assumptions or corrections, such as tests of normality and adjustment for multiple comparisons
☐	☒	A full description of the statistics including central tendency (e.g. means) or other basic estimates (e.g. regression coefficient) AND variation (e.g. standard deviation) or associated estimates of uncertainty (e.g. confidence intervals)
☐	☒	For null hypothesis testing, the test statistic (e.g. *F*, *t*, *r*) with confidence intervals, effect sizes, degrees of freedom and *P* value noted *Give P values as exact values whenever suitable.*
☒	☐	For Bayesian analysis, information on the choice of priors and Markov chain Monte Carlo settings
☒	☐	For hierarchical and complex designs, identification of the appropriate level for tests and full reporting of outcomes
☒	☐	Estimates of effect sizes (e.g. Cohen's *d*, Pearson's *r*), indicating how they were calculated
☐	☒	Clearly defined error bars *State explicitly what error bars represent (e.g. SD, SE, CI)*

Our web collection on statistics for biologists may be useful.

Software and code

Policy information about availability of computer code

Data collection	Flow cytometry data were collected using BD FACSDiva 8.0. Confocal images were acquired using Zeiss Zen-2, or Leica LAS X.
Data analysis	statistical analyses were performed with Graphpad Prism 8.3 and R 3.5.1 with the fBasics _3042.89 package; flow cytometry data analysis using BD FACSDiva 8.0 and FlowJo V10.6.1 (Treestar); confocal images were processed and analysed using Zeiss Zen-2, Leica LAS X, or rendered in 3D and analysed using Bitplane Imaris v7.7.1; electrophysiology data were acquired with pClamp 10.7 software; the quality of RNA-seq raw reads was checked using FastQC 0.11.5.; RNA-seq raw reads were trimmed using Cutadapt 2.3 and mapped to the mouse genome using TopHat 2.1.1 with Bowtie2 2.2.3.; mapped reads were quality-filtered using SAMtools 1.9.0 and quantified using HTSeq 0.9.1.; differential expression was assessed using DESeq2 1.24.0 with R 3.6.1.; gene set enrichment analysis of the filtered, DESeq2-normalized counts was performed using GSEA 4.0.3.

For manuscripts utilizing custom algorithms or software that are central to the research but not yet described in published literature, software must be made available to editors/reviewers upon request. We strongly encourage code deposition in a community repository (e.g. GitHub). See the Nature Research guidelines for submitting code & software for further information.

Data

Policy information about availability of data

All manuscripts must include a data availability statement. This statement should provide the following information, where applicable:

- Accession codes, unique identifiers, or web links for publicly available datasets
- A list of figures that have associated raw data
- A description of any restrictions on data availability

Source data files are provided with this paper. RNA sequencing data have been submitted to the NCBI Sequence Read Archive (SRA), accession number BioProject PRJNA626582.

Field-specific reporting

Please select the best fit for your research. If you are not sure, read the appropriate sections before making your selection.

☒ Life sciences ☐ Behavioural & social sciences ☐ Ecological, evolutionary & environmental sciences

For a reference copy of the document with all sections, see nature.com/authors/policies/ReportingSummary-flat.pdf

Life sciences study design

All studies must disclose on these points even when the disclosure is negative.

Sample size	Samples sizes were not pre-determined based on statistical power calculations but were based on our experience with these assays. For assays in which variability is commonly high, we typically used n>5. For assays in which variability is commonly low, we typically used n<5.
Data exclusions	No data were excluded
Replication	The experimental findings were reproduced in multiple independent experiments. The number of independent experiments and biological replicates for each data panel is indicated in the figure panel itself and in the source data files. Data in the figures represent the aggregate of all independent experiments in most cases. Data in a minority of panels are from a representative experiment (e.g. for Immunofluorescence imaging) and in those cases the number of independent experiments that reproduced the finding is also indicated in the figure legends.
Randomization	No formal randomization techniques were used; however, samples were allocated randomly to experiments and processed in an arbitrary order.
Blinding	During the Listeria treatment experiments in vivo, the mice were analyzed in a manner blinded to treatment identity. S.H. passed the de-identified mouse tissues to B.S. who performed all of the flow cytometric analyses and colony forming assays. After collecting the data, the samples were re-identified so the results could be interpreted.

Reporting for specific materials, systems and methods

Materials & experimental systems

n/a	Involved in the study
☐	☒ Unique biological materials
☐	☒ Antibodies
☒	☐ Eukaryotic cell lines
☒	☐ Palaeontology
☐	☒ Animals and other organisms
☒	☐ Human research participants

Methods

n/a	Involved in the study
☒	☐ ChIP-seq
☐	☒ Flow cytometry
☒	☐ MRI-based neuroimaging

Unique biological materials

Policy information about availability of materials

Obtaining unique materials	There are no restrictions on the availability of materials. Antibodies and chemical reagents were purchased from for-profit companies as detailed in the methods. New mouse alleles created in the course of this study (Osteolectin-CreER and Osteolectin-Tomato) will be deposited to Jackson Laboratory upon publication for distribution.

Antibodies

Antibodies used

The following antibodies were used in this study:
Anti-mouse CD2, FITC, clone RM2-5, Cat. #35-0021, LOT: C0021121118354, Tonbo, 1:200, Flow cytometry and Immunofluorescence analysis

Anti-mouse CD3, FITC, clone 17A2, Cat. #100204, LOT: B304392, BioLegend, 1:200, Flow cytometry and Immunofluorescence analysis

Anti-mouse CD5, FITC, clone 53-7.3, Cat. #100606, LOT: B210716, BioLegend, 1:200, Flow cytometry and Immunofluorescence analysis

Anti-mouse CD8a, FITC, clone 53-6.7, Cat. #35-0081, LOT: C0081100219354, Tonbo, 1:200, Flow cytometry and Immunofluorescence analysis

Anti-mouse Ter-119, FITC, clone TER-119, Cat. #116206, LOT: B272256, BioLegend, 1:200, Flow cytometry and Immunofluorescence analysis

Anti-mouse B220, FITC, clone RA3-6B2, Cat. #11-0452-86, LOT: 436128, eBiosciences, 1:200, Flow cytometry and Immunofluorescence analysis

Anti-mouse Gr-1, FITC, clone RB6-8C5, Cat. #35-5931, LOT: C5931080318354, Tonbo, 1:200, Flow cytometry and Immunofluorescence analysis

Anti-mouse c-Kit, APC-eFluor780, clone 2B8, Cat. #47-1171-82, LOT: 2018834, eBiosciences, 1:200, Flow cytometry

Anti-mouse Sca-1, PerCP-Cyanine5.5, clone D7, Cat. # 45-5981-82, LOT: 2162718, EBiosciences, 1:200, Flow cytometry

Anti-mouse CD150, BV650, clone TC15-12F12.1, Cat. #115931, LOT: B305940, BioLegend, 1:200, Flow cytometry

Anti-mouse CD48, Alexa Fluor-700, clone HM48-1, Cat. #103426, LOT: B279067, BioLegend, 1:200, Flow cytometry

Anti-mouse CD127, PE-Cyanine7, clone A7R34, Cat. #60-1271, LOT: C1271121219603, Tonbo, 1:200, Flow cytometry

Anti-mouse CD135, APC, clone A2F10, Cat. #135310, LOT: B269023, BioLegend, 1:200, Flow cytometry

Anti-mouse CD34, Biotin, clone RAM34, Cat. #13-0341-85, LOT: 2075112, eBiosciences, 1:200, Flow cytometry

Anti-mouse CD16/32, BV510, clone 93, Cat. #101333, LOT: B303788, BioLegend, 1:200, Flow cytometry

Anti-mouse CD41, Alexa Fluor-700, clone /MWReg30, Cat. #133926, LOT: B270215, BioLegend, 1:200, Flow cytometry

Anti-mouse CD105, APC, clone MJ7/18, Cat. #120414, LOT: B266785, BioLegend, 1:200, Flow cytometry

Anti-mouse Gr-1, PE-Cyanine7, clone RB6-8C5, Cat. #108416, LOT: B284962, BioLegend, 1:200, Flow cytometry

Anti-mouse CD11b, APC-eFluor780, clone M1/70, Cat. #47-0112-82, LOT: 2011193, EBiosciences, 1:200, Flow cytometry

Anti-mouse B220, PerCP-Cyanine5.5, clone RA3-6B2, Cat. #65-0452, LOT: C0452060619653, Tonbo, 1:200, Flow cytometry

Anti-mouse IgM, APC, clone 11/41, Cat. #17-5790-82, LOT: 2167008, eBiosciences, 1:200, Flow cytometry

Anti-mouse CD43, PE, clone S7, Cat. #553271, LOT: 9336727, Fisher Scientific, 1:200, Flow cytometry

Anti-mouse CD3, redFluor-710, clone 17A2, Cat. #80-0032, LOT: C0032010319803, Tonbo, 1:200, Flow cytometry

Anti-mouse Ter-119, BV510, clone TER-119, Cat. #116237, LOT: B270148, BioLegend, 1:200, Flow cytometry

Anti-mouse CD71, FITC, clone R17217, Cat. #11-0711-82, LOT: 2159109, eBiosciences, 1:200, Flow cytometry

Anti-mouse CD31, FITC, clone 390, Cat. #11-0311-82, LOT: 2086274, eBiosciences, 1:200, Flow cytometry

Anti-mouse CD24, PE-Cyanine7, clone M1/69, Cat. #101822, LOT: B250194, BioLegend, 1:200, Flow cytometry

Anti-mouse CD43, FITC, clone eBioR2/60, Cat. #11-0431-85, LOT: 1957822, eBiosciences, 1:200, Flow cytometry

Anti-mouse B220, BV510, clone RA3-6B2, Cat. #103248, LOT: B291212, BioLegend, 1:200, Flow cytometry

Anti-mouse Gr-1, BV510, clone RB6-8C5, Cat. #108438, LOT: B266530, BioLegend, 1:200, Flow cytometry

Anti-mouse CD3, APC, clone 17A2, Cat. # 20-0032-U100, LOT: C0032041219203, Tonbo, 1:200, Flow cytometry

Anti-mouse CD4, FITC, clone GK1.5, Cat.# 35-0041-U500, LOT: C0041111518354, Tonbo, 1:200, Flow cytometry

Anti-mouse CD8, PE, clone 53-6.7, Cat. # 30-0081-U500, LOT: C0081060419504, Tonbo, 1:200, Flow cytometry

Anti-mouse CD44, redFluor-710, clone IM7, Cat. # 80-0441, LOT: C0441042816803, Biolegend, 1:200, Flow cytometry

Anti-mouse CD25, PerCP-Cyanine5.5, clone PC61.5, Cat. # 65-0251-U100, LOT: C0251101518653, Tonbo, 1:200, Flow cytometry

Anti-mouse Ter-119, PE-Cyanine7, clone Ter-119, Cat. # 116222, LOT: B251241, BioLegend, 1:200, Flow cytometry

Anti-Mouse NK-1.1, PE, Clone PK136, Cat. # 557391, LOT: 09295, BD Biosciences, 1:200, Flow cytometry

Anti-mouse Leptin receptor, Biotin, Cat. #BAF497, LOT: BFV0719071, R&D Systems, 1:100, Flow; 1:200, Immunofluorescence analysis

Anti-mouse CD144, eFluor-660, clone eBioBV13, Cat. #50-1441-82, LOT: 2007696, eBiosciences, 10 ug/mouse, Flow cytometry

Anti-CD127, Alexa Fluor-647, clone A7R34, Cat. #135020, LOT: B239205, BioLegend, 2 ug/mouse, Immunofluorescence analysis

Anti-tdTomato, Cat. #632496, LOT: 1904182, Takara, 1:200, Immunofluorescence analysis

Cy3-conjugated AffiniPure Fab fragment donkey anti-rabbit IgG, Cat. #711-167-003, LOT: 145173, Jackson ImmunoResearch, 1:250, Immunofluorescence analysis

Alexa Fluor-488-conjugated AffiniPure Fab fragment donkey anti-chicken IgG, Cat. #703-546-155, LOT: 144594, Jackson ImmunoResearch, 1:250, Immunofluorescence analysis

PE-Cyanine7 streptavidin, Cat. #557598, LOT: 9011715, BD Biosciences, 1:500, Flow cytometry
PE streptavidin, Cat. #12-4317-87, LOT: 2037425, Invitrogen, 1:500, Flow cytometry

BV510 streptavidin, Cat. #405234, LOT: B258255, BioLegend, 1:500, Flow cytometry

BV421 streptavidin, Cat. #405226, LOT: B286541, BioLegend, 1:500, Flow cytometry

Anti-GFP, Cat. #GFP-1020, LOT: GFP879484, Aves, 1:200, Immunofluorescence

Alexa Fluor 555 donkey anti-goat IgG (H+L), Cat. #A32849TR, LOT: 2155590, Invitrogen, 1:250, Immunofluorescence

Alexa Fluor 647-AffiniPure F(ab')2 Fragment Donkey Anti-Rabbit IgG (H+L), Cat. #711-606-152. LOT: 143432, Jackson ImmunoResearch, 1:250, Immunofluorescence analysis

Alexa Fluor 647-AffiniPure F(ab')2 Fragment Donkey Anti-chicken IgG (H+L), Cat. #703-606-155. LOT: 143995, Jackson ImmunoResearch, 1:250, Immunofluorescence analysis

Alexa Fluor 488-AffiniPure Donkey Anti-Rabbit IgG (H+L), Cat. #711-545-152, LOT: 143957. Jackson ImmunoResearch, 1:250, Immunofluorescence analysis

Anti-CD45.1 PE-Cy7, Cat. #60-0453-U100, LOT: C0453120219603, TONBO, Flow Cytometry

Anti-CD45.2 violetFluo 450, Cat. #75-0454, LOT: C0454091819753, TONBO, Flow Cytometry

Validation

All antibodies are commercially available and have been validated in previously published studies (e.g. Nature 495:231). We have independently validated antibodies that were central to our conclusions. For instance, the anti-LepR antibody was validated using mouse bone marrow cells deficient in lepr (Cell Stem Cell 15:154).

Anti-mouse CD2. This monoclonal antibody recognizes mouse CD2. https://tonbobio.com/products/fitc-anti-mouse-cd2-rm2-5

Anti-mouse CD3. This monoclonal antibody recognizes mouse CD3. https://www.biolegend.com/en-us/products/fitc-anti-mouse-cd3-antibody-45

Anti-mouse CD5. This monoclonal antibody recognizes mouse CD5. https://www.biolegend.com/en-us/products/fitc-anti-mouse-cd5-antibody-159

Anti-mouse CD8a. This monoclonal antibody recognizes mouse CD8. https://tonbobio.com/products/fitc-anti-mouse-cd8a-53-6-7

Anti-mouse Ter-119. This monoclonal antibody recognizes mouse Ter-119. https://www.biolegend.com/en-us/products/fitc-anti-mouse-ter-119-erythroid-cells-antibody-1865

Anti-mouse B220. This monoclonal antibody recognizes mouse B220. https://www.thermofisher.com/antibody/product/CD45R-B220-Monoclonal-Antibody-RA3-6B2-FITC-eBioscience/11-0452-86

Anti-mouse Gr-1. This monoclonal antibody recognizes mouse Gr-1. https://tonbobio.com/products/fitc-anti-mouse-ly-6g-gr-1-rb6-8c5

Anti-mouse c-kit. This monoclonal antibody recognizes mouse c-kit. https://www.thermofisher.com/antibody/product/CD117-c-Kit-Antibody-clone-2B8-Monoclonal/47-1171-82

Anti-mouse Sca-1. This monoclonal antibody recognizes mouse Sca-1. https://www.thermofisher.com/antibody/product/Ly-6A-E-Sca-1-Antibody-clone-D7-Monoclonal/45-5981-82

Anti-mouse CD150. This monoclonal antibody recognizes mouse CD150. https://www.biolegend.com/en-us/products/brilliant-violet-650-anti-mouse-cd150-slam-antibody-8799

Anti-mouse CD48. This monoclonal antibody recognizes mouse CD48. https://www.biolegend.com/en-us/products/alexa-fluor-700-anti-mouse-cd48-antibody-6670

Anti-mouse CD127. This monoclonal antibody recognizes mouse CD127. https://tonbobio.com/products/pe-cyanine7-anti-mouse-cd127-il-7ra-a7r34

Anti-mouse CD135. This monoclonal antibody recognizes mouse CD135. https://www.biolegend.com/en-us/products/apc-anti-mouse-cd135-antibody-6284

Anti-mouse CD34. This monoclonal antibody recognizes mouse CD34. https://www.thermofisher.com/antibody/product/CD34-Antibody-clone-RAM34-Monoclonal/13-0341-82

Anti-mouse CD16/32. This monoclonal antibody recognizes mouse CD16/32. https://www.biolegend.com/en-us/products/brilliant-violet-510-anti-mouse-cd16-32-antibody-9917

Anti-mouse CD41. This monoclonal antibody recognizes mouse CD41. https://www.biolegend.com/en-us/products/alexa-fluor-700-anti-mouse-cd41-antibody-13058

Anti-mouse CD105. This monoclonal antibody recognizes mouse CD105. https://www.biolegend.com/en-us/products/apc-anti-mouse-cd105-antibody-6519

Anti-mouse Gr-1. This monoclonal antibody recognizes mouse Gr-1. https://www.biolegend.com/en-us/products/pe-cy7-anti-mouse-ly-6g-ly-6c-gr-1-antibody-1931

Anti-mouse CD11b. This monoclonal antibody recognizes mouse CD11b. https://www.thermofisher.com/antibody/product/CD11b-Antibody-clone-M1-70-Monoclonal/47-0112-82

Anti-mouse B220. This monoclonal antibody recognizes mouse B220. https://tonbobio.com/products/percp-cyanine5-5-anti-human-mouse-cd45r-b220-ra3-6b2

Anti-mouse IgM. This monoclonal antibody recognizes mouse IgM. https://www.thermofisher.com/antibody/product/IgM-Antibody-clone-II-41-Monoclonal/17-5790-82

Anti-mouse CD43. This monoclonal antibody recognizes mouse CD43. https://www.fishersci.com/shop/products/cd43-rat-anti-mouse-pe-clone-s7-bd/bdb553271?matchedCatNo=BDB553271&searchHijack=true&searchTerm=BDB553271&searchType=RAPID

Anti-mouse CD3. This monoclonal antibody recognizes mouse CD3. https://tonbobio.com/products/redfluor-710-anti-mouse-cd3-17a2

Anti-mouse CD71. This monoclonal antibody recognizes mouse CD71. https://www.thermofisher.com/antibody/product/CD71-Transferrin-Receptor-Antibody-clone-R17217-RI7-217-1-4-Monoclonal/11-0711-82

Anti-mouse CD31. This monoclonal antibody recognizes mouse CD31. https://www.thermofisher.com/antibody/product/CD31-PECAM-1-Antibody-clone-390-Monoclonal/11-0311-82

Anti-mouse CD24. This monoclonal antibody recognizes mouse CD24. https://www.biolegend.com/en-us/search-results/pe-cyanine7-anti-mouse-cd24-antibody-3862

Anti-mouse CD43. This monoclonal antibody recognizes mouse CD43. https://www.thermofisher.com/antibody/product/CD43-Antibody-clone-eBioR2-60-Monoclonal/11-0431-82

Anti-mouse B220. This monoclonal antibody recognizes mouse B220. https://www.biolegend.com/en-us/products/brilliant-violet-510-anti-mouse-human-cd45r-b220-antibody-7996

Anti-mouse Gr-1. This monoclonal antibody recognizes mouse Gr-1. https://www.biolegend.com/en-us/products/brilliant-violet-510-anti-mouse-ly-6g-ly-6c-gr-1-antibody-8614

Anti-mouse CD3. This monoclonal antibody recognizes mouse CD3. https://tonbobio.com/products/apc-anti-mouse-cd3-17a2

Anti-mouse CD4. This monoclonal antibody recognizes mouse CD4. https://tonbobio.com/products/fitc-anti-mouse-cd4-gk1-5

Anti-mouse CD8. This monoclonal antibody recognizes mouse CD8.

https://tonbobio.com/products/biotin-anti-mouse-cd8a-53-6-7

Anti-mouse CD44. This monoclonal antibody recognizes mouse CD44.
https://tonbobio.com/products/redfluor-710-anti-human-mouse-cd44-im7

Anti-mouse CD25. This monoclonal antibody recognizes mouse CD25.
https://tonbobio.com/products/percp-cyanine5-5-anti-mouse-cd25-pc61-5

Anti-mouse Ter-119. This monoclonal antibody recognizes mouse Ter-119.
https://www.biolegend.com/en-us/products/pe-cyanine7-anti-mouse-ter-119-erythroid-cells-antibody-3904

Anti-Mouse NK-1.1. This monoclonal antibody recognizes mouse NK-1.1.
https://www.bdbiosciences.com/us/reagents/research/antibodies-buffers/immunology-reagents/anti-mouse-antibodies/cell-surface-antigens/pe-mouse-anti-mouse-nk-11-pk136/p/557391

Anti-mouse Leptin Receptor. This monoclonal antibody recognizes mouse Leptin Receptor. https://www.rndsystems.com/products/mouse-leptin-r-biotinylated-antibody_baf497

Anti-mouse CD144. This monoclonal antibody recognizes mouse CD144. https://www.thermofisher.com/antibody/product/CD144-VE-cadherin-Antibody-clone-eBioBV13-BV13-Monoclonal/50-1441-82

Anti-CD127. This monoclonal antibody recognizes mouse CD127. https://www.biolegend.com/nl-nl/products/alexa-fluor-647-anti-mouse-cd127-il-7ralpha-antibody-6195

Anti-tdTomato. This polyclonal antibody recognizes tdTomato.

Cy3-conjugated AffiniPure Fab fragment donkey anti-rabbit IgG. This antibody reacts with rabbit IgG. It also reacts with the light chains of other rabbit immunoglobulins. No binding was detected against non-immunoglobulin serum proteins. https://www.jacksonimmuno.com/catalog/products/711-167-003

Alexa Fluor-488-conjugated AffiniPure Fab fragment donkey anti-chicken IgG. This antibody reacts with whole molecule chicken IgY. It also reacts with the light chains of other chicken immunoglobulins. No binding was detected against non-immunoglobulin serum proteins. https://www.jacksonimmuno.com/catalog/products/703-546-155

PE-Cyanine7 streptavidin. This is a second-step reagent for the indirect immunofluorescent staining of cells in combination with biotinylated primary antibodies for flow cytometric analysis. https://www.bdbiosciences.com/us/reagents/research/antibodies-buffers/second-step-reagents/avidinstreptavidin/pe-cy7-streptavidin/p/557598

PE streptavidin. This is a second-step reagent for the indirect immunofluorescent staining of cells in combination with biotinylated primary antibodies for flow cytometric analysis.
https://www.thermofisher.com/order/catalog/product/12-4317-87#/12-4317-87

BV510 streptavidin. This is a second-step reagent for the indirect immunofluorescent staining of cells in combination with biotinylated primary antibodies for flow cytometric analysis. https://www.biolegend.com/en-us/products/brilliant-violet-510-streptavidin-8140

BV421 streptavidin. This is a second-step reagent for the indirect immunofluorescent staining of cells in combination with biotinylated primary antibodies for flow cytometric analysis. https://www.biolegend.com/en-us/products/brilliant-violet-421-streptavidin-7297

Anti-GFP. This polyclonal antibody recognizes GFP.
https://www.aveslabs.com/collections/epitope-tag-6xhis-beta-gal-actin-and-gfp-antibodies/products/green-fluorescent-protein-gfp-antibody

Alexa Fluor 555 donkey anti-goat IgG (H+L). To minimize cross-reactivity, this donkey anti-goat IgG (H+L) whole secondary antibody has been affinity purified and cross-adsorbed against rabbit, rat, mouse, and human IgG.
https://www.thermofisher.com/antibody/product/Donkey-anti-Goat-IgG-H-L-Cross-Adsorbed-Secondary-Antibody-Polyclonal/A-21432

Alexa Fluor 647-AffiniPure F(ab')2 Fragment Donkey Anti-Rabbit IgG (H+L). This antibody reacts with whole molecule rabbit IgG. It also reacts with the light chains of other rabbit immunoglobulins.
https://www.jacksonimmuno.com/catalog/products/711-606-152

Alexa Fluor 647-AffiniPure F(ab')2 Fragment Donkey Anti-chicken IgG (H+L). This antibody has ensure minimal cross-reaction with bovine, goat, guinea pig, syrian hamster, horse, human, mouse, rabbit, rat and sheep serum proteins.
https://www.jacksonimmuno.com/catalog/products/703-606-155

Alexa Fluor 488-AffiniPure Donkey Anti-Rabbit IgG (H+L). This whole IgG antibody reacts with whole molecule rabbit IgG. It also reacts with the light chains of other rabbit immunoglobulins. No antibody was detected against non-immunoglobulin serum proteins.
https://www.jacksonimmuno.com/catalog/products/711-545-152

Anti-CD45.1 PE-Cy7, This monoclonal antibody recognizes mouse CD45.1
https://tonbobio.com/products/pe-cyanine7-anti-mouse-cd45-1-a20

Anti-CD45.2 violetFluo 450, This monoclonal antibody recognizes mouse CD45.2
https://tonbobio.com/products/pe-cyanine7-anti-mouse-cd45-1-a20

Animals and other organisms

Policy information about studies involving animals; ARRIVE guidelines recommended for reporting animal research

Laboratory animals	Two-month to 18-month-old C57BL/Ka mice, and 2-month-old NOD.CB17-Prkdcscid Il2rgtm1Wjl/SzJ (NSG) mice were used. Both male and female mice were used.
Wild animals	No wild animals were used.
Field-collected samples	No field-collected samples were used.

Flow Cytometry

Plots

Confirm that:

☒ The axis labels state the marker and fluorochrome used (e.g. CD4-FITC).

☒ The axis scales are clearly visible. Include numbers along axes only for bottom left plot of group (a 'group' is an analysis of identical markers).

☒ All plots are contour plots with outliers or pseudocolor plots.

☒ A numerical value for number of cells or percentage (with statistics) is provided.

Methodology

Sample preparation	Bone marrow hematopoietic cells were isolated by flushing the long bones with Ca2+- and Mg2+- free HBSS (HBSS-free) with 2% heat-inactivated bovine serum. Spleen cells were obtained by crushing the spleen between two glass slides. The cells were dissociated into a single cell suspension by gently passing them through a 25-gauge needle and then filtering through 70-um nylon mesh. For flow cytometric analysis of stromal cells, bone marrow was flushed using HBSS-free with 2% bovine serum. Then whole bone marrow was digested with type I collagenase (3mg/ml), dispase (4mg/ml) and DNase I (1U/ml) at 37°C for 30 min. Samples were then stained with antibodies and analyzed by flow cytometry.
Instrument	BD FACS Aria Fusion (for cell sorting or analysis), BD Canto (for analysis).
Software	BD FACSDiva 8.0, FlowJo V10
Cell population abundance	The abundance of the relevant cell populations within post-sort fractions was 90-100% in experiments.
Gating strategy	Mouse bone marrow stromal cells were typically isolated as cells that were positive for Leptin Receptor and negative for mouse endothelial and hematopoietic markers (mouse CD31, mouse CD45 and mouse TER119) as shown in Extended Data Fig. 1e. Mouse hematopoietic stem and progenitor cells were isolated with the gating strategies shown in Extended Data Fig. 2d. To eliminate dead cells from sorts and analyses, cells were stained with 4',6-diamidino-2-phenylindole (DAPI). The markers used for the isolation of each cell population characterized in this study are described in Extended Data Table 1,

☒ Tick this box to confirm that a figure exemplifying the gating strategy is provided in the Supplementary Information.